

# Optimising the $H\alpha$ index for the identification of activity signals in FGK stars

## Improvement of the correlation between $H\alpha$ and Ca II H&K

J. Gomes da Silva<sup>1\*</sup>, A. Bensabat<sup>1</sup>, T. Monteiro<sup>1</sup>, N. C. Santos<sup>1,2</sup>

<sup>1</sup>Instituto de Astrofísica e Ciências do Espaço, Porto, Portugal

<sup>2</sup>Departamento de Física e Astronomia, Faculdade de Ciências da Universidade do Porto, Portugal

Received XXX / Accepted XXX

### ABSTRACT

*Context.* The Ca II H&K and  $H\alpha$  lines are two of the most used activity diagnostics to detect stellar activity signals in the optical regime, and to infer about possible false positives in exoplanet detection with the radial velocity method. The flux in the two lines is known to follow the solar activity cycle, and to correlate well with sunspot number and other activity diagnostics. However, for other stars, the flux in these lines is known to have a wide range of correlations, increasing the difficulty in the interpretation of the signals observed with the  $H\alpha$  line.

*Aims.* In this work we investigate the effect of the  $H\alpha$  bandpass width in the correlation between the Ca II and  $H\alpha$  indices with the aim of improving the  $H\alpha$  index to better identify and model the signals coming from activity variability.

*Methods.* We used a sample of 152 FGK dwarfs observed with HARPS for more than 13 years with enough cadence to be able to detect rotational modulations and cycles in activity proxies. We calculated the Ca II and  $H\alpha$  activity indices using a range of bandwidths for  $H\alpha$  between 0.1 and 2.0 Å. We studied the correlation between the indices time series at long and short timescales and analysed the impact of stellar parameters, activity level and variability on the correlations.

*Results.* The correlation between Ca II and  $H\alpha$  both at short and long timespans is maximised when using narrow  $H\alpha$  bandwidths, with a maximum at 0.6 Å. For some inactive stars, as the activity level increases, the flux in the  $H\alpha$  line core increases while the flux in the line wings decreases as the line becomes shallower and broader. The balance between these fluxes can cause stars to show the negative correlations observed in the literature when using a wide bandwidth on  $H\alpha$ . These anti-correlations may become positive correlations if using the 0.6 Å bandwidth. We demonstrate that rotationally modulated signals observed in  $S_{\text{CaII}}$ , that appear flat or noisy when using 1.6 Å on  $S_{H\alpha}$ , can become more evident if a 0.6 Å bandpass is used instead. Low activity variability appears to be a contributing factor for the cases of weak or no correlations.

*Conclusions.* Calculating the  $H\alpha$  index using a bandpass of 0.6 Å maximises the correlation between Ca II and  $H\alpha$  both at short and long timescales. On the other hand, the use of the broader 1.6 Å, generally used in exoplanet detection to identify stellar activity signals, degrades the signal by including the flux in the line wings. In face to these results we strongly recommend the use of a 0.6 Å bandwidth when computing the  $H\alpha$  index for the identification of activity rotational modulation and magnetic cycle signals in solar-type stars.

**Key words.** Stars: activity – Stars: solar-type – Planets and satellites: detection – Techniques: spectroscopic

## 1. Introduction

As planet hunting instrumentation reaches higher precision levels, stellar activity becomes one of the most important limiting factors to exoplanet detection and characterization. At short timescales of days to months, rotational modulation of active regions, zones of strong magnetic fields characterized by the presence of dark and cool spots and/or bright and hotter plages, create radial velocity (RV) quasi-periodic variations with timescales close to the rotational period, its harmonics, and that of active region life times, which can be of tens of rotational periods (e.g. Saar & Donahue 1997; Queloz et al. 2001; Santos et al. 2000; Boisse et al. 2009, 2011; Santos et al. 2014; Faria et al. 2020). At longer timescales of years and decades, activity variability similar to that of the 11-year solar cycle is also known to affect

RV and can interfere with the detection of long-period planets (e.g. Lovis et al. 2011; Gomes da Silva et al. 2012).

Several techniques to correct the effects of stellar activity on RV require the simultaneous measurement of activity proxies based on activity sensitive spectral lines (or using line shape indicators) to identify and remove activity effects on RV (e.g. Boisse et al. 2011; Dumusque et al. 2012; Rajpaul et al. 2015; Faria et al. 2022). The most widely used activity sensitive lines in the optical regime are the Ca II H&K and  $H\alpha$  lines. The flux on both lines is known to correlate with the presence of active regions and both are known to follow tightly the solar magnetic cycle (Livingston et al. 2007). However, studies of time series of indices based on the two lines for other stars have shown that the correlation between the indices is not straightforward: some stars show strong positive correlations, for others the two indices are not correlated, while a few show negative correlations (Cincunegui et al. 2007; Gomes da Silva et al. 2011, 2014; Meunier et al. 2022). Although the correlation between Ca II and  $H\alpha$  is

\* e-mail: Joao.Silva@astro.up.pt

not fully understood, some studies have found that the correlation tends to be strongly positive for stars with higher activity levels, while in the low activity regime, all types of correlations are observed (Walkowicz & Hawley 2009; Gomes da Silva et al. 2011, 2014; Meunier et al. 2022).

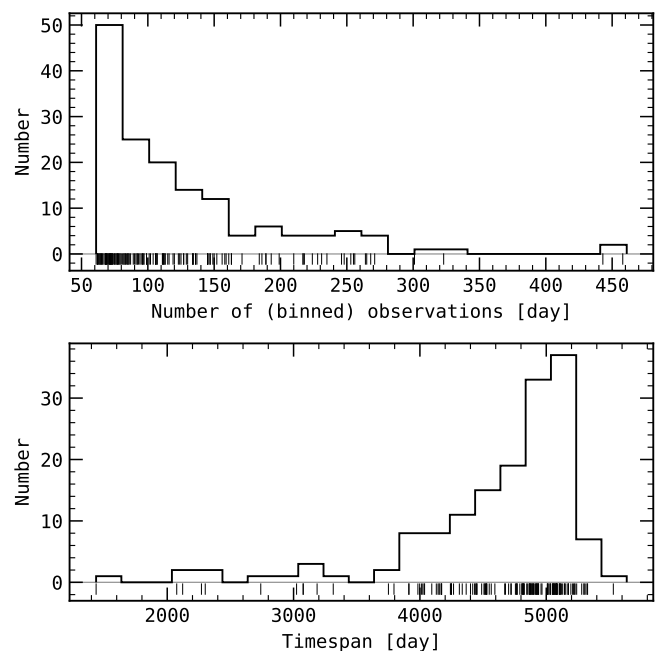
Since the cores of the Ca II H&K and H $\alpha$  lines are formed at different temperatures, and thus different heights in the chromosphere (e.g. Mauas & Falchi 1994, 1996; Mauas et al. 1997; Fontenla et al. 2016), we expect these two lines to trace activity phenomena differently. The different sensitivity of these lines to spots, plages/faculae, or filaments could explain the various correlations observed for different stars due to their varying filling factors, spatial distribution and/or contrasts (e.g. Meunier & Delfosse 2009). Although some previous works have used a narrow bandpass of 0.678 Å to compute H $\alpha$  (e.g. Kürster et al. 2003; Bonfils et al. 2007; Boisse et al. 2009; Santos et al. 2010), the majority of the recent studies of stellar activity, mainly in the context of exoplanet detection, have used broader bandwidths, usually of 1.6 Å. In fact, most studies of the correlation between Ca II and H $\alpha$ , for FGK stars or the Sun, have also used a broad bandwidth to measure the H $\alpha$  index (Cincunegui et al. 2007; Gomes da Silva et al. 2014; Maldonado et al. 2019; Meunier et al. 2022).

In this work we analyse the effect of changing the H $\alpha$  bandpass width on the correlation between the flux in the Ca II and H $\alpha$  lines with the aim of maximising the correspondence between the two activity diagnostics and increase the H $\alpha$  sensitivity to stellar signals at short and long timescales. To our knowledge, this is the first time the impact of changing the bandwidth size of the H $\alpha$  index is analysed for stars other than the Sun. In §2 we present our sample and in §3 we explain how we calculated the Ca II and H $\alpha$  indices. In §4 we expose our methodology to determine the correlation coefficients and their significance. We analyse the long-term correlations between Ca II and H $\alpha$  in §5 and the short-term correlations in §6. A discussion of the results in terms of stellar parameters, activity variability, and an analysis of the H $\alpha$  line wings is presented in §7, and we conclude in §8.

## 2. Sample and HARPS data

The sample was selected from the Gomes da Silva et al. (2021) catalogue of chromospheric activity of 1 674 FGK stars from the HARPS (Mayor et al. 2003) archive. This catalogue used more than 180 000 spectra to estimate precise and homogeneous mean activity levels and dispersion. The catalogue also includes stellar atmospheric parameters such as effective temperature, metallicity and surface gravity along with isochronal masses, radii and ages. The High Accuracy Radial Velocity Planet Searcher (HARPS) is a high-resolution, high-stability, fibre-fed, cross-dispersed echelle spectrograph with a resolution of  $\lambda/\Delta\lambda = 115\,000$  and a spectral range from 380 nm to 690 nm, mounted at the ESO 3.6 m telescope in La Silla, Chile. For a detailed description of the instrument we refer to Pepe et al. (2002).

The main objective of the present work involves the comparison of the activity signals measured in the flux of the Ca II and H $\alpha$  lines, and therefore our timespan and cadence needs to cover the rotational modulation and activity cycles related variability for each star, if possible. To achieve this we need stars with high number of observations and long timespans. We therefore selected from the catalogue main sequence FGK stars with more than 60 days of observations and timespans longer than



**Fig. 1.** Distribution of number of observations (upper panel) and timespan (lower panel) per star.

1 000 days. As we will see in §6 and can be observed in Fig. B.1, this selection enabled us to identify activity minima and maxima in magnetic cycles for most stars, and to have enough data points to use those epochs to compare the behaviour of our activity indices. Since some stars have very high cadences, characteristic of asteroseismology surveys, we imposed a maximum limit of 1 000 spectra per star to reduce computational costs. Outliers were removed via a sequential 4-sigma clipping of the  $S_{\text{Ca II}}$ ,  $S_{\text{H}\alpha 16}$ , and  $S_{\text{H}\alpha 06}$  indices time series (these indices are explained in §3 and §4). Since we are only interested in timescales longer than one day, all data was daily binned to mitigate high frequency noise (Dumusque et al. 2011) and reduce the datasets. This selection resulted in a sample of 152 FGK dwarfs, including 101 G, 33 K and 18 F stars, with a total of 19 019 binned data points. Figure 1 shows the distributions of the number of binned observations and timespan per star. The number of binned observations per star range between 61 and 458 with the median at 101, and the timespan ranges from 1 437 days (3.9 years) to 5 531 days (15.1 years) with the median at 4 865 days (13.3 years).

We also obtained stellar atmospheric parameters such as effective temperature,  $T_{\text{eff}}$ , metallicity, [Fe/H], and median chromospheric emission ratio,  $\log R'_{\text{HK}}$ , from Gomes da Silva et al. (2021) and references therein. The distribution of these parameters for the sample are shown in Fig. 2 and their values provided in Table C.1. The effective temperature varies between 4 470 and 6 732 K, with the median at 5 694 K, the metallicity between  $-1.39$  and  $0.33$  dex, with the median at  $-0.11$  dex, and  $\log R'_{\text{HK}}$  ranges from  $-5.13$  to  $-4.60$  dex, with the median at  $-4.93$  dex. Thus, the majority of our sample stars have about 100 days of observation on a timespan of almost 5 000 days ( $\sim 13.7$  yr), and have effective temperature and activity levels similar to our Sun, with slightly sub-solar metallicity. These biases are due to the majority of these stars coming from exoplanet surveys targeting inactive, solar-type stars. Nevertheless, we should be

able to assess the influence of these stellar parameters on the behaviour of the activity indices, if they are present.

### 3. Activity indices based on the Ca II H&K and H $\alpha$ lines

We used ACTIN<sup>1</sup> (Gomes da Silva et al. 2018, 2021) to calculate the Ca II and H $\alpha$  indices for the full sample. ACTIN calculates indices by integrating the flux in the activity sensitive lines and dividing them by the flux in pseudo-continuum regions:

$$I = \frac{\sum_i^N F_i}{\sum_j^M R_j} \quad (1)$$

where  $F_i$  is the flux in the activity line  $i$ ,  $N$  is the number of activity lines (e.g. for Ca II  $N = 2$ , for H $\alpha$   $N = 1$ ),  $R_j$  is the flux in the pseudo-continuum region  $j$ , and  $M$  the number of pseudo-continuum regions. Generally there two pseudo-continuum regions ( $M = 2$ ) surrounding the activity lines in the redder and bluer nearby continuum. ACTIN uses linear interpolation to deal with the finite wavelength resolution of the spectrograph when integrating the flux over a given bandpass. For more information related to the flux determination and errors we refer to Gomes da Silva et al. (2021, Appendix A).

The Ca II index, which comes preinstalled in ACTIN, was measured following the procedure in Gomes da Silva et al. (2021) which mimics the original Mt. Wilson  $S$ -index derivation by Vaughan et al. (1978). In the case of H $\alpha$ , we used the reference lines from Gomes da Silva et al. (2011) but computed the index for a range of central bandwidths between 0.1 and 2.0 Å, in steps of 0.1 Å. Since we are not comparing the values of these indices between different stars, only the correlations between them, the temperature dependent photospheric contribution and bolometric correction are not required. To compare the activity levels of stars we use the usual  $\log R'_{\text{HK}}$  indicator (Noyes et al. 1984; Rutten 1984). From now on we will refer to the spectral lines as Ca II and H $\alpha$ , and to the indices as  $S_{\text{Ca II}}$  and  $S_{\text{H}\alpha}$ .

### 4. Correlation coefficients and significance

As a metric for correlation we choose the Spearman coefficient over the Pearson so that we can infer correlations that are monotonic, either linear or not. Furthermore, the Spearman coefficient does not require the two datasets to be normally distributed, as is the case where we have correlated time series with signals such as the quasi-periodic modulation due to activity. The Spearman correlation coefficient,  $\rho$ , was calculated for  $S_{\text{Ca II}}$  and each  $S_{\text{H}\alpha}$  using a different bandwidth. To quantify the correlation significance, we calculated the  $p$ -value of the coefficients following the methodology described in Figueira et al. (2013)<sup>2</sup>. Briefly, for each star, we performed 10 000 Fisher-Yates shuffling of the data pairs ( $S_{\text{Ca II}}$  and  $S_{\text{H}\alpha}$ ) to create unbiased and uncorrelated datasets, for which we calculated the correlation coefficients. The original correlation coefficient (before shuffling) was then compared with the mean of the shuffled population correlation coefficients, and the original dataset  $z$ -score was calculated. The  $p$ -value, the probability of having an equal or larger correlation coefficient under the null hypothesis that the data pairs are uncorrelated, was obtained from the one-sided probability of having such a  $z$ -score from the observed Gaussian distribution.

<sup>1</sup> <https://github.com/gomesdasilva/ACTIN>

<sup>2</sup> A python implementation of the algorithm is available at <https://bitbucket.org/pedrofigueira/line-profile-indicators/src/master/>.

To compare values of the coefficients for narrow and wide bands we use two representative bandwidths. As referred to in the introduction, the most used H $\alpha$  bandwidth to calculate the H $\alpha$  index is the 1.6 Å bandpass. Due to its widespread use, we will consider it as an example of a wide bandpass, and will refer to this index as  $S_{\text{H}\alpha 16}$  from now on. As a reference to a narrow bandwidth we will use the H $\alpha$  index calculated by integrating a 0.6 Å bandwidth, referred to as  $S_{\text{H}\alpha 06}$ <sup>3</sup>. For computational cost reasons, we only calculated the  $p$ -values for correlations using  $S_{\text{H}\alpha 06}$ ,  $S_{\text{H}\alpha 16}$ , and  $S_{\text{H}\alpha W}$  (this last index is discussed in §7.3) both for the long- and short-term datasets.

From now on, we refer to "strong" correlations if  $\rho$  has values higher than 0.5 in absolute value, and "weak or no correlation" if  $\rho$  has values between  $-0.5$  and  $0.5$ . For example, we can have strong correlations that are insignificant ( $p$ -value  $\geq 10^{-3}$ ) or weak correlations that are significant ( $p$ -value  $\leq 10^{-3}$ ). As we will see in the following sections, for the long-term datasets all the strong correlations are significant, however that is not always true for the short-term datasets.

## 5. Long-term correlations

To investigate the correlation between  $S_{\text{Ca II}}$  and  $S_{\text{H}\alpha}$  in at long timescales we used the full time series for all stars. The Spearman correlation coefficients and their  $p$ -values when using bandpass widths of 0.6 and 1.6 Å as well as using the H $\alpha$  line wings between 1.6 and 0.6 Å (see §7.3) are provided in Table C.2.

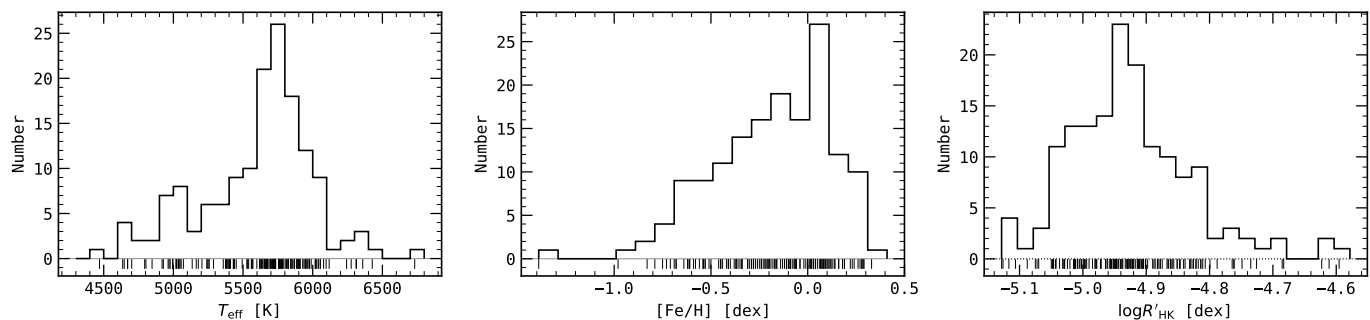
### 5.1. Correlations for different H $\alpha$ bandwidths

We expect the correlation between Ca II and H $\alpha$  to vary with the H $\alpha$  bandwidth used because different depths of the H $\alpha$  line probe different heights of the stellar atmosphere.

Figure 3 shows the Spearman correlation coefficients as a function of H $\alpha$  bandwidth coloured after activity level. In the upper panel we show only stars having strong positive or negative correlations ( $\rho \geq 0.5$  and  $\rho \leq -0.5$ ) using the 0.6 Å bandwidth as an example of a narrow bandpass, while in the lower panel only stars with weak or no correlations ( $-0.5 < \rho < 0.5$ ) with  $S_{\text{H}\alpha 06}$  are represented. In the case of  $S_{\text{H}\alpha 06}$  and  $S_{\text{H}\alpha 16}$ , all stars with  $|\rho| \geq 0.5$  also have  $p$ -values  $\leq 10^{-3}$ , meaning that all those correlations are statistically significant. On a first observation, we see a tendency for the correlation to decrease as the H $\alpha$  bandwidth increases. Four different behaviours of the correlation as a function of bandwidth can be observed: (1) "flat-positive", where the correlation is strong positive and almost constant across bandwidths, (2) "positive-zero", where it decreases from strong positive to weak or no correlation, (3) "positive-negative", where it decreases from strong positive to strong negative, and (4) "flat-negative", where it is constant but always strong negative. The figure also provides other interesting information:

- All cases of strong positive  $S_{\text{Ca II}}-S_{\text{H}\alpha 16}$  correlation also have strong positive  $S_{\text{Ca II}}-S_{\text{H}\alpha 06}$  correlation (upper panel) – there are no cases where the correlation increases from weak to strong with increasing bandpass width.
- All cases of strong negative  $S_{\text{Ca II}}-S_{\text{H}\alpha 16}$  correlation have strong positive  $S_{\text{Ca II}}-S_{\text{H}\alpha 06}$  correlation, except for HD 206998 (upper panel) – narrow bandpasses can turn strong anti-correlations into strong positive correlations.

<sup>3</sup> As we will see in §5.2 this is the bandwidth that maximises the correlation between  $S_{\text{Ca II}}$  and  $S_{\text{H}\alpha}$ .



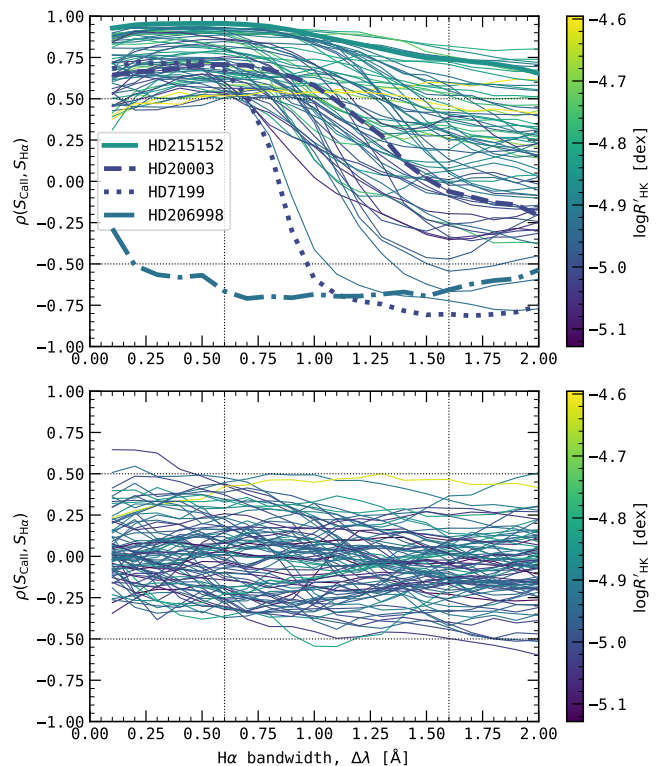
**Fig. 2.** Distribution of effective temperature (left panel), metallicity (middle panel), and  $\log R'_{\text{HK}}$  activity level (right panel) for our sample.

- All cases of weak or no correlation between  $S_{\text{CaII}}$  and  $S_{\text{H}\alpha 06}$  also show weak or no correlation between  $S_{\text{CaII}}$  and  $S_{\text{H}\alpha 16}$  (lower panel) – these stars never show strong correlations between the calcium and hydrogen lines regardless of the  $\text{H}\alpha$  bandwidth used.
- The only case of strong negative  $S_{\text{CaII}}-S_{\text{H}\alpha 06}$  correlation, HD 206998, also has strong negative  $S_{\text{CaII}}-S_{\text{H}\alpha 16}$  correlation (upper panel) – since we only have one star in this situation we can not ascertain whether this is an outlier or an additional "behaviour".
- In general, stars with lower correlations with  $S_{\text{H}\alpha 16}$  tend to have lower activity levels (upper panel) – in agreement with Gomes da Silva et al. (2014); Meunier et al. (2022).

These behaviours show that, for most inactive<sup>4</sup> FGK dwarfs, using a narrow  $\text{H}\alpha$  bandpass can improve the correlation between the  $\text{H}\alpha$  and  $\text{Ca II}$  indices, and that most of the anti-correlations detected between these two indices are caused by using a wide bandwidth when calculating the  $\text{H}\alpha$  index. It is also interesting to note that if a star has no correlation using  $S_{\text{H}\alpha 06}$ , then widening the bandpass will not improve the correlation into either strong positive or negative values. In general terms, narrower bandwidths are preferred if one wants to detect activity signals similar to those followed by  $\text{Ca II}$  (which is known to correlate well with plages in the Sun and with activity induced radial velocity).

In Fig. 4 we show three examples of the  $\text{H}\alpha$  profile for three cases represented in Fig. 3 (upper panel) in which all have similar  $S_{\text{CaII}}-S_{\text{H}\alpha 06}$  correlation coefficients but behave differently as the  $\text{H}\alpha$  bandwidth is increased. To compare the  $\text{H}\alpha$  lines at maxima and minima we normalised the spectra by the mean of the flux in the  $R_1$  and  $R_2$  pseudo-continuum regions used to compute the  $S_{\text{H}\alpha}$  index. The left panel shows HD 215152 (K3V), a star with a "flat-positive" behaviour, in the middle panel we show HD 20003 (G8V), a star showing "positive-zero" behaviour, and in the right panel HD 7199 (G9V) an example of a "positive-negative" correlation behaviour. The top panels show the  $\text{H}\alpha$  line at the minimum (blue) and maximum (red) of  $S_{\text{CaII}}$  activity for each star while the bottom panels show the difference in flux between these extremes. The vertical lines in all figures represent the limits of the 0.6 Å bandwidth (dotted lines), the 1.6 Å (dashed lines), and the maximum bandwidth value we used of 2.0 Å (solid lines). The numbers in the lower panels show the flux difference calculated in each width, coloured red if positive (more flux at activity maximum) and blue if negative (more flux at activity minimum). The first thing we can observe in these examples is that the flux in the core always increases with  $S_{\text{CaII}}$  activity level, while the flux in the wings can increase or decrease

<sup>4</sup> Active stars are known to have strong positive correlations between  $S_{\text{CaII}}$  and  $S_{\text{H}\alpha}$



**Fig. 3.** Effect of varying the  $\text{H}\alpha$  bandwidth in the correlation between  $\text{Ca II}$  and  $\text{H}\alpha$  coloured after activity level measured as  $\log R'_{\text{HK}}$ . *Upper panel:* Stars with strong positive ( $\rho \geq 0.5$ ) or negative ( $\rho \leq -0.5$ ) correlation with the  $S_{\text{H}\alpha 06}$  index. Stars marked with thick lines are examples used in Figs. 4, 7, and A.2, and the only case of negative correlation with  $S_{\text{H}\alpha 06}$  (HD 206998). *Lower panel:* Stars with weak or no correlation ( $-0.5 < \rho < 0.5$ ) with the  $S_{\text{H}\alpha 06}$  index. In both panels, as an indication, we mark the boundaries between strong and no correlation with horizontal dotted lines at  $\rho$  values of 0.5 and  $-0.5$  with vertical dotted lines.

with activity level. We can see that for the case of HD 215152 (left panel), as  $\text{Ca II}$  increases, both the  $\text{H}\alpha$  line core (between the 0.6 Å limits) and the lateral "wings" of the lines increase in flux. Thus, the correlation between  $\text{Ca II}$  and  $\text{H}\alpha$  is positive, either if using a narrow or a wider bandpass. On the other hand, in the case of HD 20003 (middle panel), while the difference in flux in the line core is positive as the activity increases, the line wings widen and thus decrease in flux, producing a negative flux difference. This means that, while we get a positive correlation using a narrowband, as we increase the bandwidth, we start degrading

the correlation by including the negative flux difference from the line wings, and the correlation drops to almost zero because the positive flux difference in the core and the negative flux difference in the wings almost compensate each other. If the broadening (the drop in flux) of the H $\alpha$  wings is larger than the increase in flux in the core, like in the case of HD 7199 (right panel), the correlation can become negative when a wide bandpass is used. However, a strong positive correlation is still possible if a narrow bandwidth is used instead. A similar H $\alpha$  profile behaviour was previously observed by Flores et al. (2016, 2018) while studying the activity cycles of the two solar analogs HD 45184 and HD 38858 (both included in our sample). While the H $\alpha$  equivalent width showed no significant variability, the shape of the H $\alpha$  profile produced variations compatible with the Ca II cyclic variations. In fact, their H $\alpha$  profile core (<0.7 Å from centre) increased in flux with Ca II activity level while the "wings" flux decreased.

## 5.2. H $\alpha$ bandwidth that maximises correlations

Now that we have a strong indication that narrower bandwidths tend to improve the Ca II-H $\alpha$  correlation, we are going to determine which bandpass maximises it.

For each star, we selected the bandwidth for which the correlation coefficient,  $\rho$ , has maximum *absolute* value, thus maximising either positive or negative correlations. Figure 5 shows the distribution of bandpasses that maximise the correlation, where the black histogram shows the bandpass distribution for stars for which the maximum absolute  $\rho$  never passes the strong correlation threshold, the blue hatched and red histograms shows the bandpass distribution for stars for which the maximum  $\rho$  is either strong positive or negative, respectively. For the 152 stars in this sample we found an equal number of stars with strong positive and weak or no correlations, 72 (47.4%), while only 8 stars (5.3%) show strong negative correlations. The black histogram shows that there is a weak tendency for the bandpasses that maximise the correlation between the two indices to have narrower widths even though the correlation is never strong. When we select only the maximum strong correlations, either positive (blue hatched) or negative (red) it becomes clear that using narrower filters between around 0.4 and 0.6 Å maximises the cases of strong positive correlations between H $\alpha$  and Ca II, while the few cases of strong anti-correlations (negative) appear preferably when using wider > 1.0 Å H $\alpha$  bandpasses. This maximisation process tends to prefer narrow bandpasses when the H $\alpha$  wings flux behaves in such a way that it will compensate the flux changes in the core, and therefore including the wings will degrade the correlation coefficient absolute value, while it prefers wider bandpasses when the wings flux variation is larger than that of the core, thus having more importance when the line flux is fully integrated.

To identify the bandwidth that maximises the strong positive Ca II-H $\alpha$  correlation we calculated the number of stars with a correlation coefficient higher than 0.5 for each H $\alpha$  bandwidth (Fig. 6). The best bandwidth,  $\Delta\lambda = 0.6$  Å, was selected as the one including more stars. The number of stars with strong positive correlation using 0.6 Å is 69 (45%) while using the widely used 1.6 Å bandpass is just 20 (13%). Even though the optimal bandwidth is 0.6 Å, any bandwidth between around 0.25 and 0.75 Å have similar results. Beyond ~0.75 Å, the number of stars with strong positive correlations starts to decline significantly, and those bandwidths should not be used to integrate the H $\alpha$  flux for the  $S_{H\alpha}$  index.

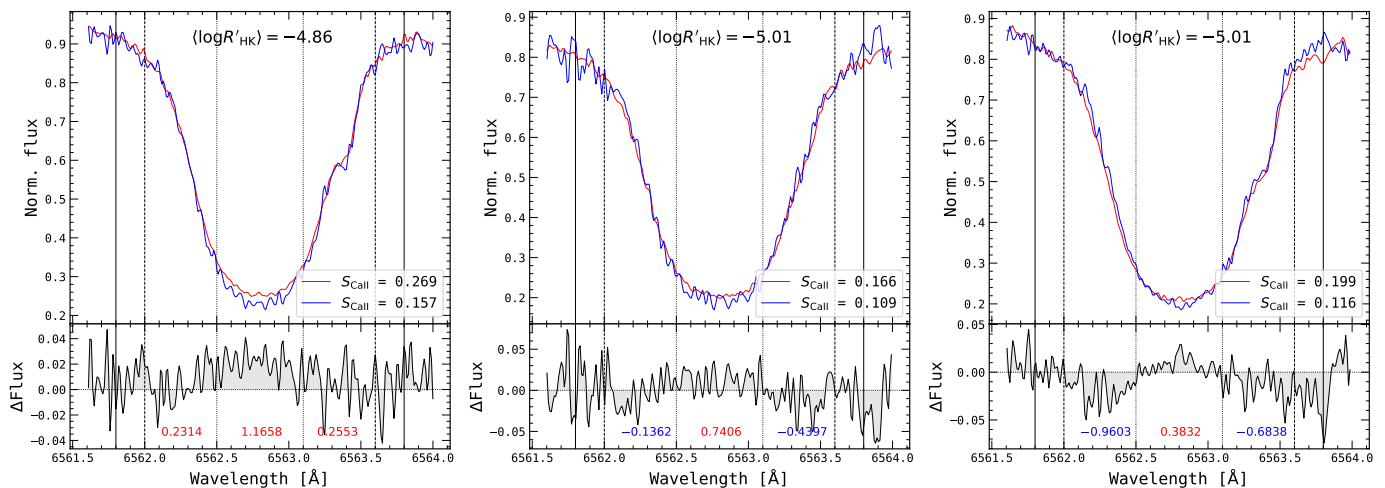
As an example of the benefits of using a 0.6 Å bandwidth instead of 1.6 Å to follow long-term activity we show in Fig. 7 the time series of the three stars used as example in Figs. 3 and 4, namely HD 215152, HD 20003, and HD 7199, using  $S_{CaII}$ ,  $S_{H\alpha16}$ , and  $S_{H\alpha06}$  which show strong positive, no correlation, and strong negative correlations between  $S_{CaII}$  and  $S_{H\alpha16}$ , respectively. This shows that using  $S_{H\alpha06}$  can increase the positive correlation observed in  $S_{H\alpha16}$  (top panels), turn no correlations (and an apparent flat signal) into a strong positive correlation with an obvious cycle pattern (middle panel), and turn a strong negative correlation (an "anti-cycle") into a strong positive correlation (a cycle, lower panel). Two of these stars (HD 215152 and HD 7199) were used in Meunier et al. (2022, Fig. 5) in their study of the correlation between the  $S_{CaII}$  and  $S_{H\alpha}$  indices as examples of positive and negative correlations for their  $S_{H\alpha}$  using 1.6 Å.

## 6. Short-term correlations

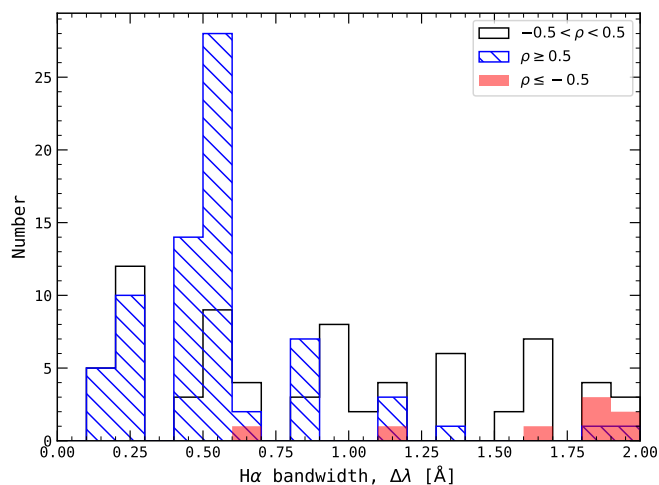
After arriving to the conclusion that the bandwidth of 0.6 Å maximises the correlation between Ca II and H $\alpha$  for long timescales, we are now interested in assessing what happens in the short-term, more characteristic of the timescales of stellar rotation. Furthermore, we are interested to see how is the behaviour of the H $\alpha$  index, using wide or narrow bandwidths, when the stars are at the maximum and minimum of their activity cycles. To achieve this, we need to identify the epochs of activity minima and maxima in the time series and then calculate the correlation coefficient between the  $S_{CaII}$  and  $S_{H\alpha06}$  and Ca II and  $S_{H\alpha16}$  indices for these epochs. Main sequence FGK stars have rotation periods that range from <1 day to around 60-70 days, depending on their ages (McQuillan et al. 2014), while the magnetic cycles of these types of stars are of the orders of years to decades (Baliunas et al. 1995). We therefore need to select the maxima and minima epochs with timespans long enough to be able to cover the range of rotation periods of these stars while being short enough to isolate the maxima of activity from the minima and to exclude the effect of long-term variations associated with magnetic cycles. The maxima and minima epochs were identified using the following methodology:

1. Grouped the  $S_{CaII}$ ,  $S_{H\alpha06}$ , and  $S_{H\alpha16}$  time series into a grid of 30 day steps. This value, close to the higher envelope of the rotation periods of FGK dwarfs (McQuillan et al. 2014, Fig. 1), is enough to cover most of the rotation periods in just one grid step.
2. Each epoch was defined as a group of points surrounded by empty steps, so that, for example, two (30 day) consecutive steps surrounded by two empty (30 day) steps would constitute an epoch (with a 60 days step).
3. Only epochs with at least seven observations were considered to ensure we have minimum points to calculate correlation coefficients.
4. The epoch with the highest  $S_{CaII}$  mean value is the epoch at the activity maximum, while the epoch with the lowest  $S_{CaII}$  mean is the activity minimum.
5. To ensure that the activity levels of the maximum and minimum epochs are well separated in activity level, we imposed that the difference between the means of each epoch is at least two times the average standard deviations of the two epochs:  $\langle S_{CaII,max} \rangle - \langle S_{CaII,min} \rangle \geq 2(\sigma(S_{CaII,max}), \sigma(S_{CaII,min}))$ .

This resulted in 103 stars with well separated epochs of activity maxima and minima. The timespans obtained for the maxima

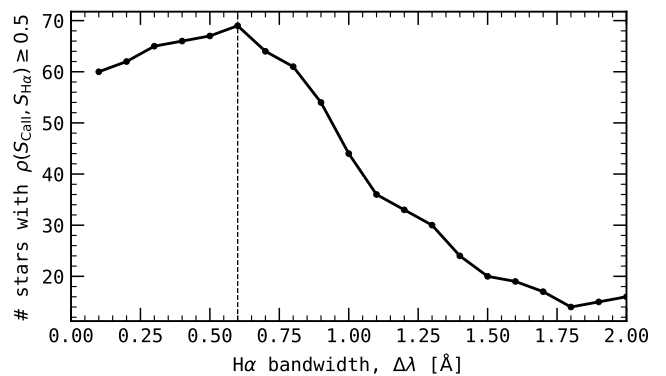


**Fig. 4.** *Upper panels:*  $H\alpha$  line profiles of HD 21512 (left), HD 20003 (middle), and HD 7199 (right) at their maxima (red) and minima (blue) activity levels. *Lower panels:* Difference between the fluxes at maximum and minimum of activity for each star. Vertical lines show bandwidths of 2.0 Å (solid), 1.6 Å (dashed), and 0.6 Å (dotted). The numbers in the lower panels show the integrated flux difference in each region delimited by the vertical lines in red if positive and blue if negative.



**Fig. 5.** Distribution of bandpasses that maximise the correlation between  $H\alpha$  and  $Ca II$ . The black histogram shows the bandpass distribution for stars with weak or no correlation coefficient ( $-0.5 < \rho < 0.5$ ), the blue hatched histogram shows stars with strong positive correlations ( $\rho \geq 0.5$ ) and the red histogram stars with strong negative correlations ( $\rho \leq -0.5$ ).

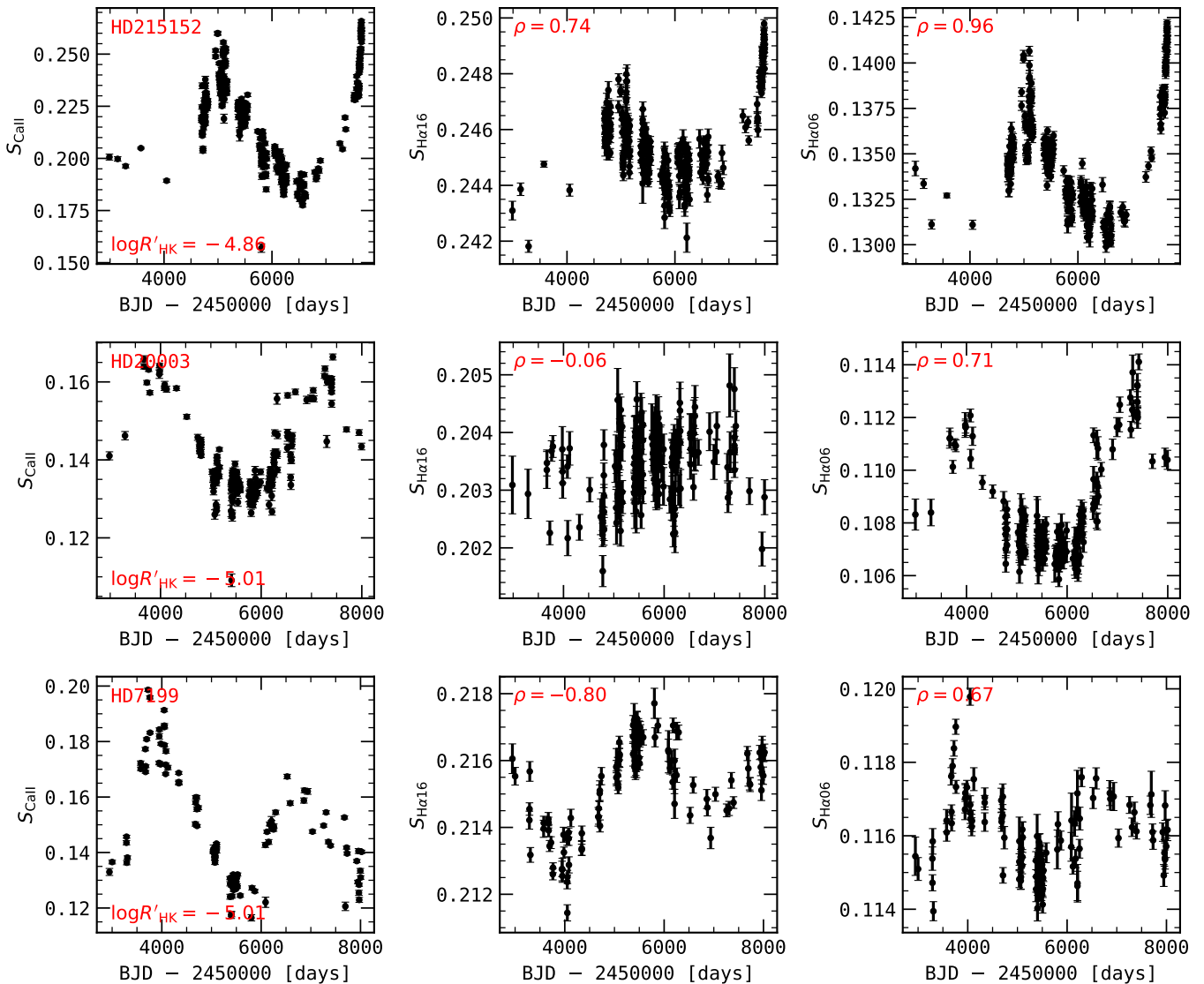
and minima epochs range between 6 and 238 days, with the median at 88 days. The  $S_{Ca II}$  time series for these stars, with the maxima and minima identified with red and blue points, respectively, are provided in the Appendix B. After completing this selection process we calculated the Spearman correlation coefficients between  $S_{Ca II}$  and  $S_{H\alpha 06}$ , and  $S_{H\alpha 16}$ , and their respective  $p$ -values, for the maximum and minimum epochs of each star. The correlation coefficients along with  $p$ -values and mean and standard deviation of  $S_{Ca II}$  for the full sample (before applying point 5 of the above selection) are provided in Table C.3. Contrary to the case of the long-term correlations in §5, not all stars with  $|\rho| \geq 0.5$  have  $p$ -values  $\leq 10^{-3}$ , which means that there are cases of strong correlations that are not statistically significant. This is probably a consequence of the reduced number of data



**Fig. 6.** Number of stars with correlation coefficient between  $Ca II$  and  $H\alpha$  greater than 0.5 (strong positive correlation) for different bandwidths. The vertical dashed line indicates the maximum at  $\Delta\lambda = 0.6$  Å.

points in these datasets when compared to the full datasets used in the long-term analysis.

Figure 8 presents the distribution of the correlation coefficients between  $S_{Ca II}$  and  $S_{H\alpha}$  at maxima (red line) and minima (black dashed line) for the cases of  $S_{H\alpha 06}$  (top panel) and  $S_{H\alpha 16}$  (bottom panel). The correlations with significant coefficients ( $p$ -value  $\leq 10^{-3}$ ) are represented by the red filled histograms for the activity maxima and black hatched histograms for the activity minima. The first thing to note is that the only cases of significant correlations, for both  $S_{H\alpha 06}$  and  $S_{H\alpha 16}$ , are positive correlations with  $\rho$  close to or above 0.5. There are more cases of strong positive correlations ( $\rho \geq 0.5$ ) at maximum than at minimum of activity for both  $H\alpha$  indices, while there are more cases of strong negative correlations ( $\rho \leq -0.5$ ) at minimum than at maximum. Similarly to the long-term case, using the 0.6 Å bandwidth in  $H\alpha$  maximises the number of stars with strong positive correlation with the calcium lines, both for epochs at maximum and minimum of activity, however the number of significant ( $p$ -values  $\leq 10^{-3}$ ) at minimum (black hatched histogram) is the same for the two indices.



**Fig. 7.**  $S_{\text{CaII}}$ ,  $S_{\text{H}\alpha 16}$ , and  $S_{\text{H}\alpha 06}$  for HD 215152 (top panels), HD 20003 (middle panels), and HD 7199 (lower panels).

Out of the 103 stars analysed, 50 (49%) show strong positive correlations between  $S_{\text{CaII}}$  and  $S_{\text{H}\alpha 06}$  at activity maximum (15, 15%, having  $p$ -value  $\leq 10^{-3}$ ), while 23 (22%) have strong positive correlation at activity minimum (1, 1%, having  $p$ -value  $\leq 10^{-3}$ ). There are no cases of significant negative correlations between  $S_{\text{CaII}}$  and  $S_{\text{H}\alpha 06}$  at maximum or minimum of activity. In comparison, when using  $S_{\text{H}\alpha 16}$ , only 26 (25%) showed strong positive correlations (7, 7%, with  $p$ -value  $\leq 10^{-3}$ ) at activity maximum and 14 (14%) at activity minimum (1, 1%, with  $p$ -value  $\leq 10^{-3}$ ). The figure also shows that at these shorter timescales there are more cases of anti-correlations both at minimum and maximum of activity for  $S_{\text{H}\alpha 06}$ . We should note, however, that we are using considerably fewer data points to compute the correlations at short timescales, and this will influence the significance of the correlation coefficients as demonstrated by the reduced number of cases with  $p$ -values below  $10^{-3}$ .

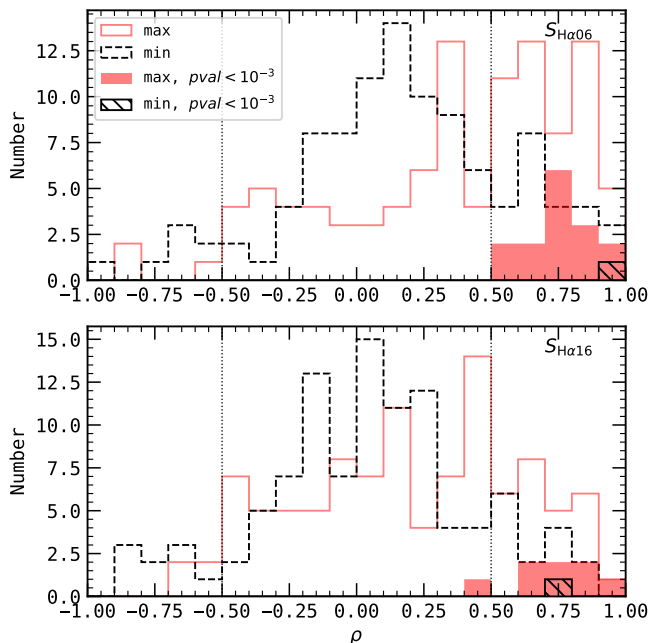
An example of the improvement of using the narrower bandwidth also at short timescales is given in Fig. 9 where we show the rotational modulation of the K dwarf HD 109200 as measured by  $S_{\text{CaII}}$  (upper panel),  $S_{\text{H}\alpha 06}$  (middle panel), and  $S_{\text{H}\alpha 16}$  (lower panel), selected at a region close to the activity cycle max-

imum. As can be observed, the  $S_{\text{H}\alpha 06}$  signal closely follows the modulation observed in  $S_{\text{CaII}}$  while the signal from  $S_{\text{H}\alpha 16}$  appears to degrade the modulation signal. This has implications for the detection of rotation periods of stars when using the H $\alpha$  time series. If a wide H $\alpha$  bandwidth is used, the rotational modulation could be degraded, diminishing the significance of the signal. In the case of RV analysis in the context of exoplanet detection, this could increase the rate of false positives, by failing to identify activity signals, their harmonics and aliases.

## 7. Discussion

### 7.1. Trends with effective temperature, metallicity and activity level

Although using a 0.6 Å bandwidth maximises the correlation between  $S_{\text{CaII}}$  and  $S_{\text{H}\alpha}$ , there are still about half of the stars which show weak or no correlation. To understand why, we searched for clues by analysing the correlation coefficient between  $S_{\text{CaII}}$ ,  $S_{\text{H}\alpha 06}$  and  $S_{\text{H}\alpha 16}$  against the stellar parameters effective temperature, metallicity and the activity level measured by  $\log R'_{\text{HK}}$ .

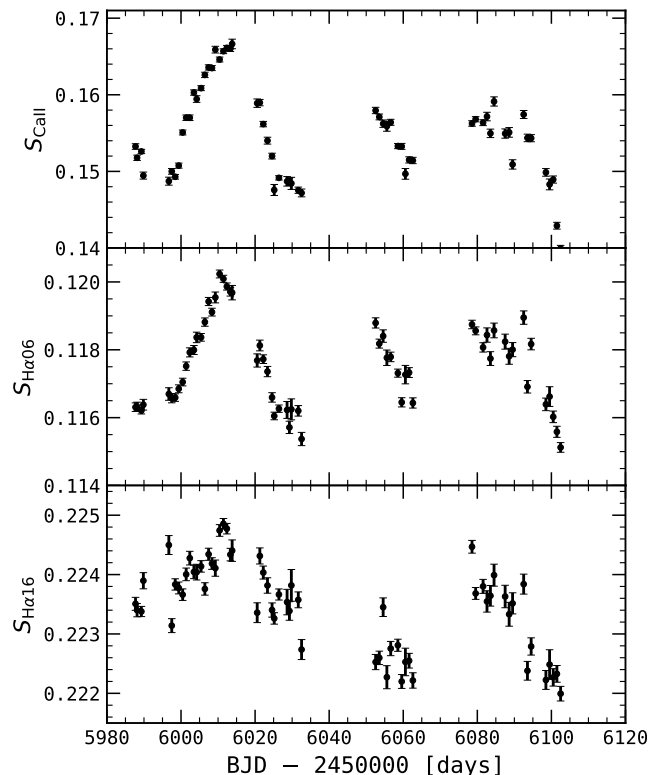


**Fig. 8.** Distribution of the correlation coefficient between  $S_{\text{CaII}}$  and  $S_{\text{H}\alpha 06}$  (upper panel) and  $S_{\text{CaII}}$  and  $S_{\text{H}\alpha 16}$  (lower panel). The red histograms are the coefficients for epochs at the maximum of activity ( $p$ -value  $\leq 10^{-3}$ , filled red) while the black histograms are the coefficients for epochs at minimum ( $p$ -value  $\leq 10^{-3}$ , hatched black).

The top panel of Fig. 10 shows that there is no trend of the  $S_{\text{CaII}}-S_{\text{H}\alpha 16}$  correlation (red squares) with effective temperature. This was also observed by Gomes da Silva et al. (2014) and Meunier et al. (2022) using a 1.6 Å H $\alpha$  bandpass. However, when using  $S_{\text{H}\alpha 06}$  as the H $\alpha$  index (black circles) we see that almost all K dwarfs ( $T_{\text{eff}} < 5250$  K) have strong positive correlations, while hotter F and G stars have strong positive ( $\rho \geq 0.5$ ), weak or no correlations ( $-0.5 \leq \rho \leq 0.5$ ), and strong negative correlations ( $\rho \leq -0.5$ ).

In the middle panel, when using  $S_{\text{H}\alpha 16}$  (red squares) there is a tendency for the strong negative correlations ( $\rho \leq -0.5$ ) to be present at higher metallicity values, as was previously observed by Gomes da Silva et al. (2014). This trend disappears when using  $S_{\text{H}\alpha 06}$  (black circles), meaning that the correlation between  $S_{\text{CaII}}$  and  $S_{\text{H}\alpha 06}$  is not related to the metal content of stars.

The impact of the Ca II activity level in the  $S_{\text{CaII}}-S_{\text{H}\alpha 16}$  correlation was already observed for FGK dwarfs by Gomes da Silva et al. (2014) and Meunier et al. (2022) and for M dwarfs by Walkowicz & Hawley (2009) and Gomes da Silva et al. (2011), where more active stars have a tendency to show strong positive correlations, while negative and weak or no correlations appear preferably for inactive stars. The bottom panel shows this tendency is present when using  $S_{\text{H}\alpha 16}$  (red squares). However, for a narrow bandpass on H $\alpha$  (black circles), we find that the strong positive correlations can be present for a greater number of inactive stars, including those with  $\log R'_{\text{HK}}$  levels below  $-5.0$  dex. There is also no strong negative correlations when using  $S_{\text{H}\alpha 06}$  (except one possible outlier). The correlation between  $S_{\text{CaII}}$  and  $S_{\text{H}\alpha 06}$  seems to be independent on the activity level of the stars.



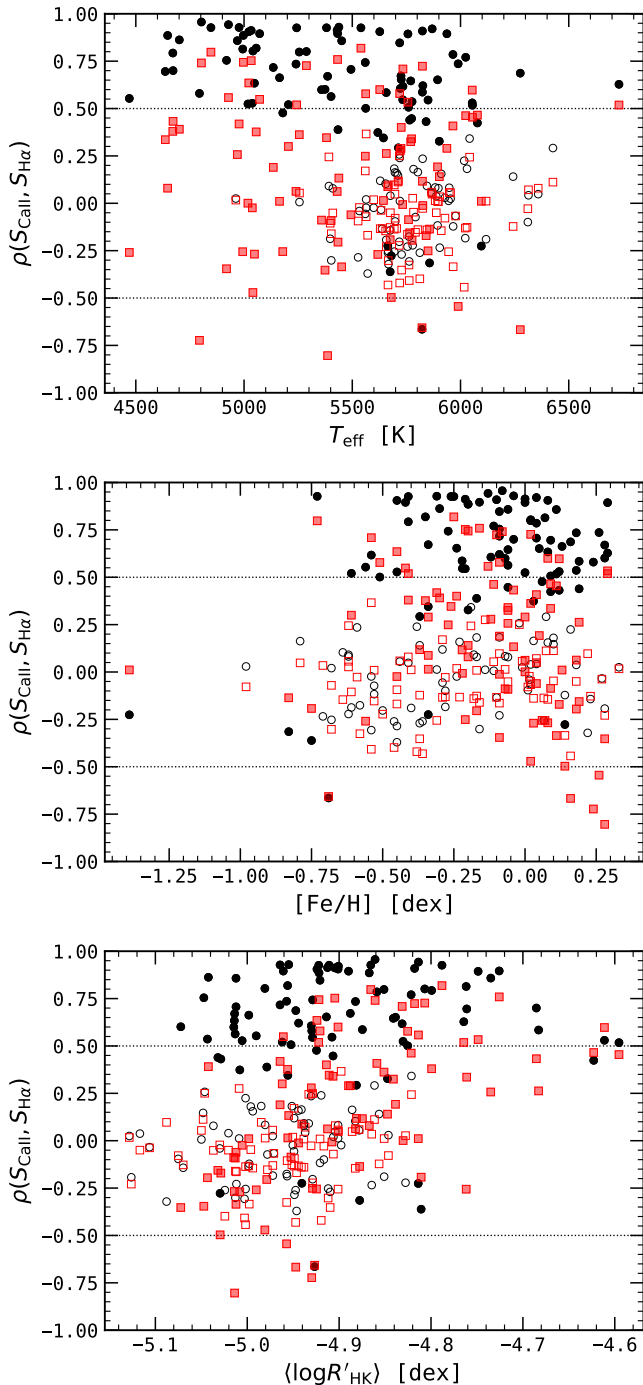
**Fig. 9.** Rotational modulation near the activity cycle maximum of HD 109200 measured by the  $S_{\text{CaII}}$  (upper panel),  $S_{\text{H}\alpha 06}$  (middle panel), and  $S_{\text{H}\alpha 16}$  (lower panel) activity indices.

## 7.2. The effect of activity variability

Gomes da Silva et al. (2021) studied the chromospheric activity of FGK stars and found that the vast majority of the K dwarfs in their sample (including stars and observations used here) have high  $\log R'_{\text{HK}}$  variability even though they are considered inactive, with  $\log R'_{\text{HK}} < -4.75$  dex. The authors also observed that F and G inactive dwarfs can have both low and high variability and that FGK dwarfs with activity levels above around  $-4.8$  dex tend to have high variability. We therefore suspect that the explanation for the lack of stars with weak or no correlation for higher activity levels ( $\log R'_{\text{HK}} > -4.8$  dex) and for K dwarfs ( $T_{\text{eff}} < 5250$  K) might be the same: high activity variability. To test this, we plotted the activity variability-level diagram with a 2D density map from the Gomes da Silva et al. (2021) catalogue using just main sequence stars and overplotted the stars from this sample using squares for stars with strong positive correlation ( $\rho \geq 0.5$ ) and inverted triangles for stars with weak or no, or negative correlation ( $\rho < 0.5$ ), coloured after their  $\rho$  value, as shown in Fig. 11. As we can see, the majority of the stars with strong positive correlation have high activity variability (with  $\log(\sigma_{R_s}) > -1.4$  dex) while the stars with weak or no correlation have low variability. Furthermore, activity level is not a main factor for strong positive correlations between  $S_{\text{CaII}}$  and  $S_{\text{H}\alpha 06}$ , since they are present in both inactive and active stars, as can also be observed in Fig. 10, lower panel.

Figure 11 also shows why we found previously that almost all K dwarfs have strong positive correlations (right panel) while some FG dwarfs show weak or no correlations (left panel): almost all K dwarfs have high activity variability while F and G dwarfs show a greater range in variability that reach lower





**Fig. 10.** Spearman correlation coefficient between  $S_{\text{CaII}}$  and  $S_{\text{H}\alpha 06}$  (black circles) and  $S_{\text{CaII}}$  and  $S_{\text{H}\alpha 16}$  (red squares) against effective temperature (top panel), metallicity (middle panel), and median  $\log R'_{\text{HK}}$  activity level (bottom panel). Horizontal dotted lines mark the thresholds for strong correlations at  $\rho = 0.5$  and  $-0.5$ . Filled markers are significant correlations with  $p$ -value  $\leq 10^{-3}$ .

amplitudes. This shows that, instead of activity level, the Ca II variability (here measured by the logarithm of the dispersion of  $R_5 = 10^5 \times R'_{\text{HK}}$ ) is one of the main contributions for the correlation between Ca II and  $S_{\text{H}\alpha 06}$ .

### 7.3. The H $\alpha$ wings

In the previous sections we showed that the inclusion of flux from the H $\alpha$  wings in the  $S_{\text{H}\alpha}$  index increases the number of strong negative correlations between  $S_{\text{CaII}}$  and  $S_{\text{H}\alpha}$ , and deteriorates the activity signals, especially for stars with lower activity levels and higher metal content. To inspect the behaviour of the H $\alpha$  wings with  $S_{\text{CaII}}$  activity, we constructed a new index,  $S_{\text{H}\alpha\text{W}}$ , using the flux of H $\alpha$  considering a bandpass with limits between those of 1.6 and 0.6 Å. The Spearman correlation coefficient between  $S_{\text{CaII}}$  and  $S_{\text{H}\alpha\text{W}}$  and the corresponding  $p$ -values were calculated according to the methodology described in §4.

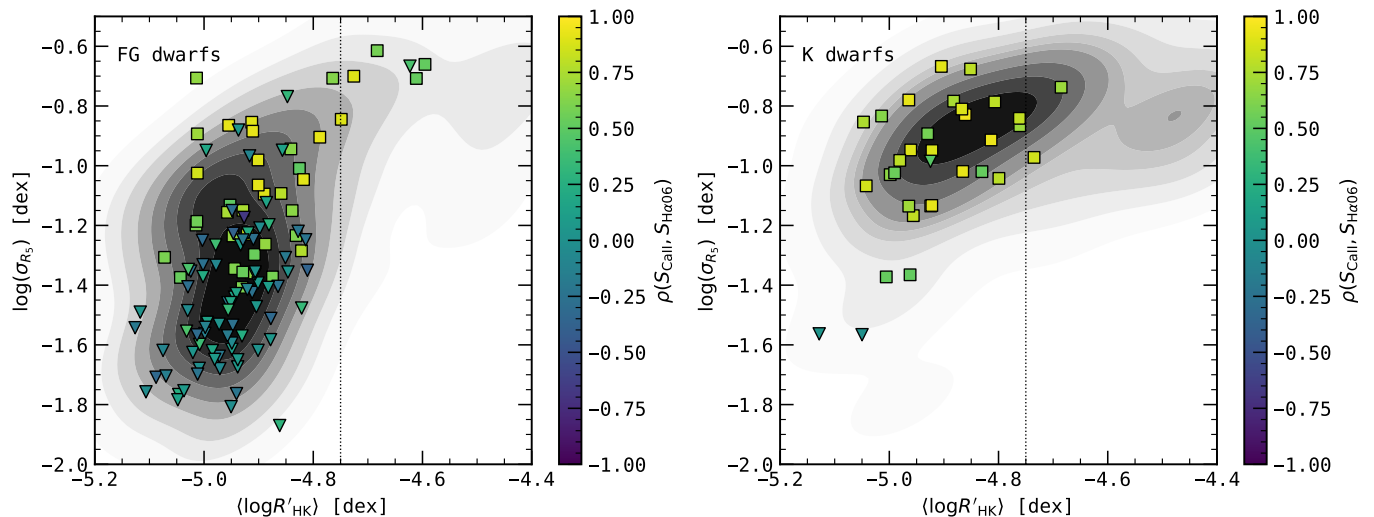
Most of the significant correlations between  $S_{\text{H}\alpha\text{W}}$  and  $S_{\text{CaII}}$  are negative and these are present mainly for inactive stars with  $\log R'_{\text{HK}}$  below around  $-4.9$  dex and stars with higher metallicity (Fig. A.1). This behaviour explains the anti-correlations between  $S_{\text{CaII}}$  and  $S_{\text{H}\alpha 16}$  in inactive stars (Gomes da Silva et al. 2014; Meunier et al. 2022) and also the tendency for these to be present in higher metallicity stars (Gomes da Silva et al. 2014). Interestingly, there are also a few stars with positive correlations between  $S_{\text{CaII}}$  and  $S_{\text{H}\alpha\text{W}}$ , with  $\rho$  close to 0.5. These stars are typically G dwarfs with higher activity levels than the ones with negative correlations.

Figure A.2 shows the comparison between the time series of  $S_{\text{CaII}}$ ,  $S_{\text{H}\alpha 16}$  and  $S_{\text{H}\alpha\text{W}}$  for the same stars used before to exemplify the three different behaviours of the H $\alpha$  index when compared to  $S_{\text{CaII}}$ . For HD 215152 (upper panels), we saw in Fig. 7 that both the  $S_{\text{H}\alpha 06}$  and  $S_{\text{H}\alpha 16}$  indicators were positively correlated with  $S_{\text{CaII}}$ , with  $S_{\text{H}\alpha 06}$  having a stronger correlation coefficient than  $S_{\text{H}\alpha 16}$ . Here we see that the index based solely on the H $\alpha$  wings flux has a very weak correlation with  $S_{\text{CaII}}$ , which explains the  $S_{\text{H}\alpha 16}$  correlation being weaker than that of the core-based  $S_{\text{H}\alpha 06}$ . In the case of HD 20003 (middle panels), there is a strong anti-correlation between  $S_{\text{CaII}}$  and  $S_{\text{H}\alpha\text{W}}$ , which contributes to the mitigation of the strong positive correlation observed for  $S_{\text{H}\alpha 06}$  in Fig. 7 and results in a non-correlation for  $S_{\text{H}\alpha 16}$ . In the case of HD 7199 (lower panels), the variation of flux with activity in the wings is higher (in negative values) than that of the core, as we saw in Fig. 4, turning the positive correlation between  $S_{\text{CaII}}$  and  $S_{\text{H}\alpha 06}$  observed in Fig. 7 into a strong anti-correlation when the wings flux is added in  $S_{\text{H}\alpha 16}$ .

Following these results, we can explain the correlation between  $S_{\text{H}\alpha}$  and H $\alpha$  based on the balance between the flux in the core and that of the wings:

- The flux in the H $\alpha$  line core appears to be always (except for cases of low activity variability) positively correlated to that of the Ca II H&K lines.
- The flux in the H $\alpha$  line wings has a tendency to be negatively correlated to that of the Ca II H&K lines., mainly in inactive and higher metallicity stars.
- When the flux in the H $\alpha$  line wings is included in the derivation of the  $S_{\text{H}\alpha}$  index, there will be strong negative correlations with the Ca II H&K lines for inactive and higher metallicity stars when the variation of flux with activity in the wings is stronger than that of the H $\alpha$  core. For the more active stars ( $\log R'_{\text{HK}} > -4.8$  dex) the flux variation in the wings is irrelevant when compared to that of the core, producing a strong positive correlation.

Since the Ca II H&K lines are known to be well correlated with the presence of plages/faculae this indicates that the core of the H $\alpha$  line is following the same phenomena. The existence of strong (negative) correlations between the flux in the H $\alpha$  line



**Fig. 11.** Stellar activity variability measured as  $\log(\sigma_{R_5})$  versus median activity level,  $(\log R'_{\text{HK}})$ , for our sample coloured after the Spearman correlation coefficient between  $S_{\text{CaII}}$  and  $S_{\text{H}\alpha 06}$ . Left panel are FG dwarfs while the right panel shows K dwarfs. Squares are stars with  $\rho \geq 0.5$  (strong positive correlations) while inverted triangles stars with  $\rho < 0.5$ . The gray scale map shows the Bivariate Kernel Density Estimate (KDE) from the catalogue of [Gomes da Silva et al. \(2021\)](#) using just the main sequence stars of the selected spectral types of each panel. The vertical dotted line at  $\log R'_{\text{HK}} = -4.75$  dex marks the original Vaughan-Preston gap ([Vaughan & Preston 1980](#)), separating the active and inactive stars.

wings and Ca II H&K shows that the wings contain activity information. [Meunier & Delfosse \(2009\)](#) discussed the contributions of plages and filaments to the flux in the H $\alpha$  line, showing that the contribution of plages would produce a positive correlation between the flux in Ca II and H $\alpha$ , while filaments would contribute to a negative correlation, and thus, the combination of plages and filaments could result in non-correlations or anti-correlations depending on the plages and filaments filling factors, contrasts, and/or distributions (see also [Meunier et al. 2022](#)). It seems that, by separating the H $\alpha$  line core from the line wings, we could be observing those behaviours separately, meaning that the flux in the H $\alpha$  wings could be following the presence of filaments in the stellar disk. However, the identification of the structures responsible for the observed correlations is beyond the scope of the present work. Further investigation could be carried out by obtaining high-resolution spectra of different resolved activity structures in the Sun to analyse the H $\alpha$  profile and compare the flux in the H $\alpha$  line, measured with different bandwidths with the presence of specific activity features. This could be done e.g. with the future PoET Solar telescope ([Santos et al. in prep.](#)) to be installed at Paranal, Chile, and connected to the ESPRESSO spectrograph ([Pepe et al. 2021](#)).

## 8. Conclusions

In this work we analysed the effect of varying the H $\alpha$  bandwidth on the correlation between the  $S_{\text{CaII}}$  and  $S_{\text{H}\alpha}$  activity indices using a sample of FGK stars observed with HARPS with cadence and long timespans enough to detect rotation and cycle induced variability. We also compared the activity signals coming from long-term cycles and short-term rotation modulation using representative bandwidths: a narrow (0.6 Å), wide (1.6 Å) bandpasses, and also a bandpass using just the line wings (1.6 – 0.6 Å).

While studying the correlations between  $S_{\text{CaII}}$  and  $S_{\text{H}\alpha}$  for long- and short-timescales we found in general similar results. However the statistical significance is stronger for the long-

timescales case, probably due to the increased number of data points used.

The effect of changing the H $\alpha$  bandwidth for the correlation between  $S_{\text{CaII}}$  and  $S_{\text{H}\alpha}$  can be summarised as follows:

- Narrower bandwidths have a tendency for strong positive correlations with  $S_{\text{CaII}}$ .
- Wider bandwidths result in a great variety of correlations.
- There are no cases where the correlation is stronger when using a wider bandwidth than using a narrower.
- Narrow bandwidths can convert some strong negative correlations observed with wider bands to strong positive correlations.
- The bandwidth that maximises positive correlations with  $S_{\text{CaII}}$  is 0.6 Å.

Previous works investigating the correlation between  $S_{\text{CaII}}$  and  $S_{\text{H}\alpha}$  for FGK dwarfs using wide bandwidths, generally of 1.6 Å, have found that the correlation between  $S_{\text{CaII}}$  and  $S_{\text{H}\alpha}$  depends on activity level and metallicity, where for low activity levels and higher metallicity there are non- and negative correlations and for higher activity levels the correlations are strong positive ([Gomes da Silva et al. 2014](#); [Meunier et al. 2022](#)). They also found that the correlation is not dependent on the effective temperature of stars. In this work we arrived at the same results. However, when analysing the correlations using a narrower bandpass of 0.6 Å we found that most stars have strong positive correlations, independently of activity level and metallicity. Furthermore, the cause for non correlations appears to be low activity variability.

We also analysed an index based on the flux of the H $\alpha$  wings, and studied its correlation with  $S_{\text{CaII}}$ . We found that the behaviour is similar to that of the H $\alpha$  index with the wide 1.6 Å bandpass, but without strong positive correlations and with more cases of strong negative correlations.

Regarding the time series, we observed that both long-term activity cycle variations and short-term rotation modulated variations are better followed by  $S_{\text{H}\alpha}$  if using the narrower 0.6 Å bandwidth, mainly for inactive and K dwarfs.

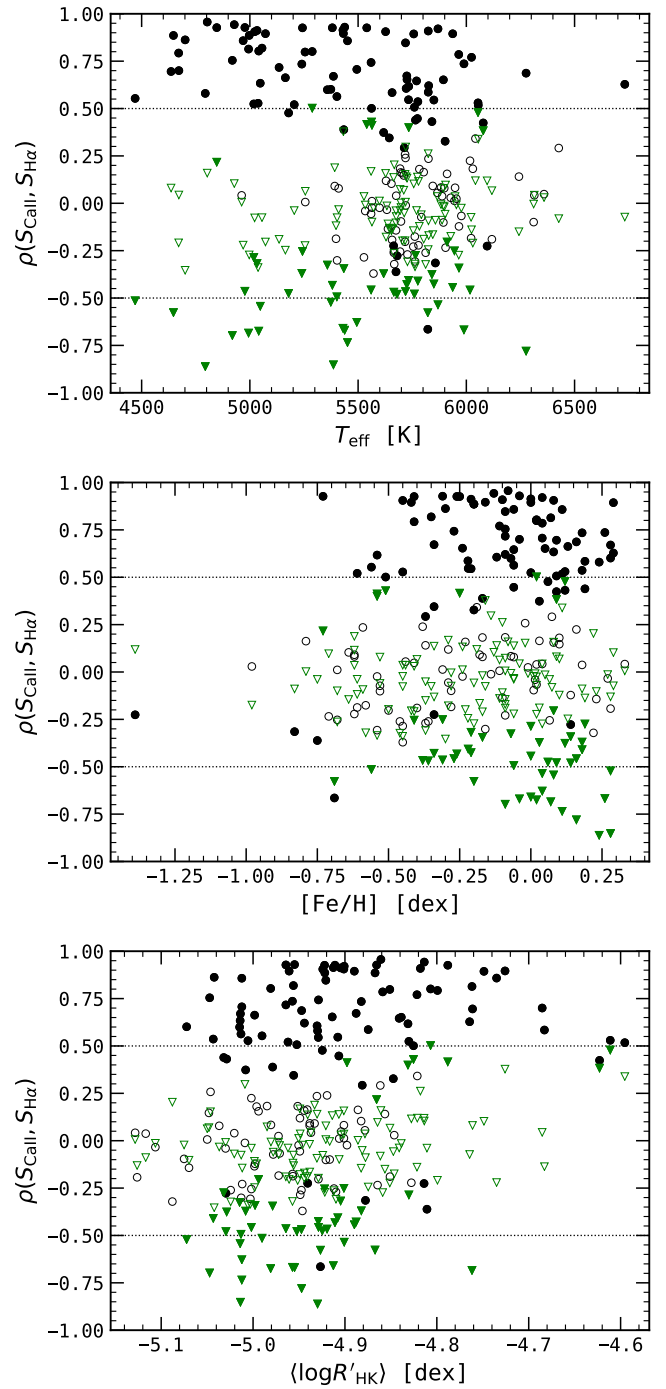
In conclusion, the correlation between  $S_{\text{CaII}}$  and  $S_{\text{H}\alpha 16}$  depends on the balance between the flux variation with activity between the line core and line wings of H $\alpha$ . While the H $\alpha$  line core is positively correlated with  $S_{\text{CaII}}$ , the H $\alpha$  wings show signs of following activity that is generally anti-correlated with the line core. This kind of H $\alpha$  profile behaviour was previously observed for two solar analogs by Flores et al. (2016, 2018) where they suggested that the H $\alpha$  index should be constructed taking into account the profile variations instead of the integrated flux in the line. Here, we suggest a simple alternative solution by integrating the flux in a narrower bandwidth covering only the line core, which is able to achieve similar results.

Having demonstrated that the widely used 1.6 Å bandwidth on H $\alpha$  degrades the quality of activity signals both at long and short timescales, we recommend the use of a narrower bandwidth, around 0.6 Å or between  $0.25 \geq \Delta\lambda \geq 0.75$  Å, when calculating the H $\alpha$  index to better identify both rotationally modulated and magnetic cycle activity signals and to decrease false positives when identifying activity with the H $\alpha$  for radial-velocity exoplanet searches.

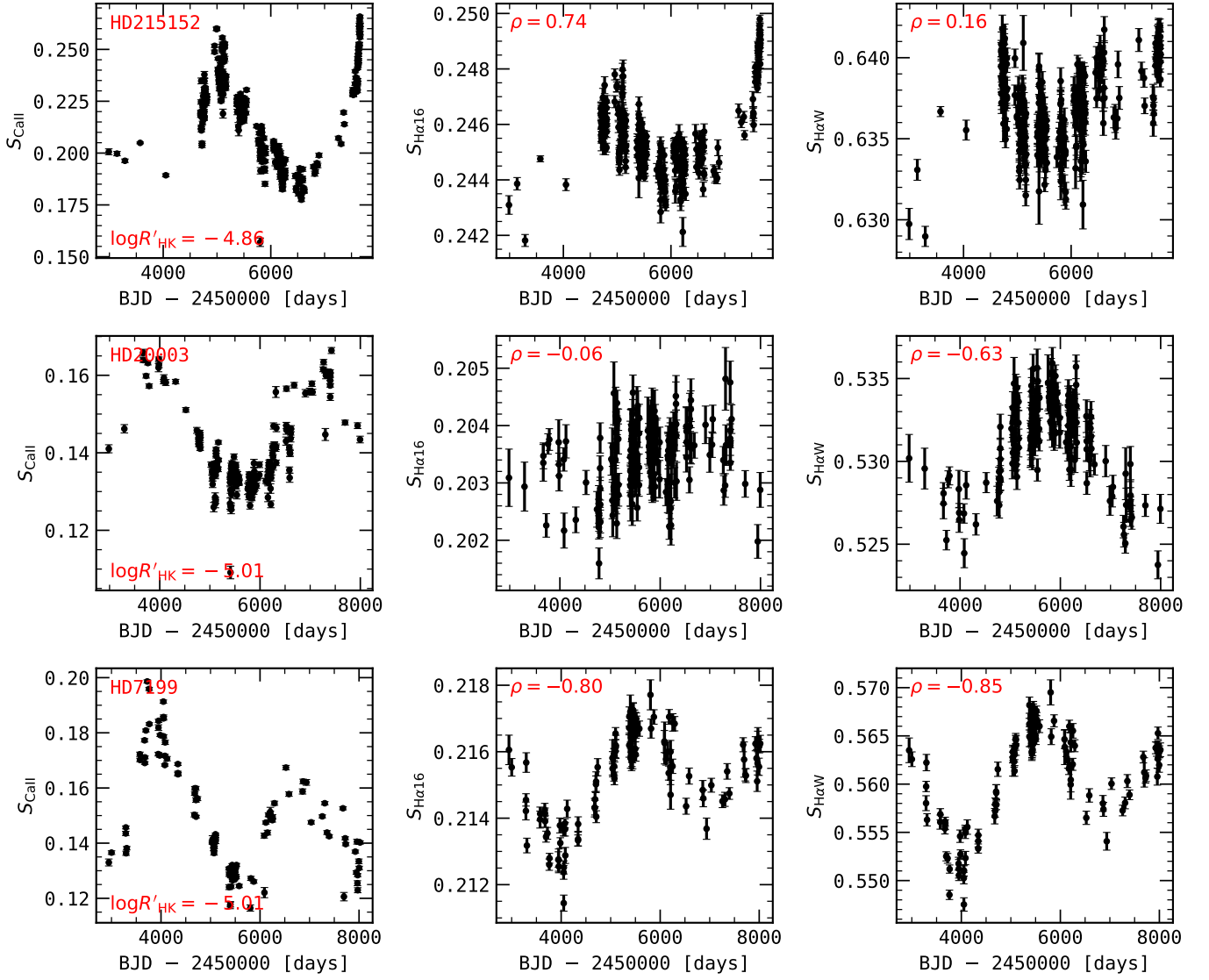
*Acknowledgements.* This work was supported by FCT - Fundação para a Ciência e a Tecnologia through national funds and by FEDER through COMPETE2020 - Programa Operacional Competitividade e Internacionalização by these grants: UIDB/04434/2020 & UIDP/04434/2020; PTDC/FIS-AST/32113/2017 & POCI-01-0145-FEDER-032113; PTDC/FIS-AST/28953/2017 & POCI-01-0145-FEDER-028953.

## References

- Baliunas, S. L., Donahue, R. A., Soon, W. H., et al. 1995, ApJ, 438, 269
- Boisse, I., Bouchy, F., Hébrard, G., et al. 2011, A&A, 528, A4+
- Boisse, I., Moutou, C., Vidal-Madjar, A., et al. 2009, A&A, 495, 959
- Bonfils, X., Mayor, M., Delfosse, X., et al. 2007, A&A, 474, 293
- Cincunegui, C., Díaz, R. F., & Mauas, P. J. D. 2007, A&A, 469, 309
- Dumusque, X., Pepe, F., Lovis, C., et al. 2012, Nature, 491, 207
- Dumusque, X., Udry, S., Lovis, C., Santos, N. C., & Monteiro, M. J. P. F. G. 2011, A&A, 525, A140+
- Faria, J. P., Adibekyan, V., Amazo-Gómez, E. M., et al. 2020, A&A, 635, A13
- Faria, J. P., Suárez Mascareño, A., Figueira, P., et al. 2022, A&A, 658, A115
- Figueira, P., Santos, N. C., Pepe, F., Lovis, C., & Nardetto, N. 2013, A&A, 557, A93
- Flores, M., González, J. F., Jaque Arancibia, M., Buccino, A., & Saffe, C. 2016, A&A, 589, A135
- Flores, M., González, J. F., Jaque Arancibia, M., et al. 2018, A&A, 620, A34
- Fontenla, J. M., Linsky, J. L., Witbrod, J., et al. 2016, ApJ, 830, 154
- Gomes da Silva, J., Figueira, P., Santos, N., & Faria, J. 2018, The Journal of Open Source Software, 3, 667
- Gomes da Silva, J., Santos, N. C., Adibekyan, V., et al. 2021, A&A, 646, A77
- Gomes da Silva, J., Santos, N. C., Boisse, I., Dumusque, X., & Lovis, C. 2014, A&A, 566, A66
- Gomes da Silva, J., Santos, N. C., Bonfils, X., et al. 2011, A&A, 534, A30+
- Gomes da Silva, J., Santos, N. C., Bonfils, X., et al. 2012, A&A, 541, A9
- Kürster, M., Endl, M., Rouesnel, F., et al. 2003, A&A, 403, 1077
- Livingston, W., Wallace, L., White, O. R., & Giampapa, M. S. 2007, ApJ, 657, 1137
- Lovis, C., Dumusque, X., Santos, N. C., et al. 2011, ArXiv e-prints [arXiv:1107.5325]
- Maldonado, J., Phillips, D. F., Dumusque, X., et al. 2019, A&A, 627, A118
- Mauas, P. J. D. & Falchi, A. 1994, A&A, 281, 129
- Mauas, P. J. D. & Falchi, A. 1996, A&A, 310, 245
- Mauas, P. J. D., Falchi, A., Pasquini, L., & Pallavicini, R. 1997, A&A, 326, 249
- Mayor, M., Pepe, F., Queloz, D., et al. 2003, The Messenger, 114, 20
- McQuillan, A., Mazeh, T., & Aigrain, S. 2014, ApJS, 211, 24
- Meunier, N. & Delfosse, X. 2009, A&A, 501, 1103
- Meunier, N., Kretschmar, M., Gravet, R., Mignon, L., & Delfosse, X. 2022, A&A, 658, A57
- Noyes, R. W., Hartmann, L. W., Baliunas, S. L., Duncan, D. K., & Vaughan, A. H. 1984, ApJ, 279, 763
- Pepe, F., Cristiani, S., Rebolo, R., et al. 2021, A&A, 645, A96
- Pepe, F., Mayor, M., Rupprecht, G., et al. 2002, The Messenger, 110, 9
- Queloz, D., Henry, G. W., Sivan, J. P., et al. 2001, A&A, 379, 279
- Rajpaul, V., Aigrain, S., Osborne, M. A., Reece, S., & Roberts, S. 2015, MNRAS, 452, 2269
- Rutten, R. G. M. 1984, A&A, 130, 353
- Saar, S. H. & Donahue, R. A. 1997, ApJ, 485, 319
- Santos, N. C., Gomes da Silva, J., Lovis, C., & Melo, C. 2010, A&A, 511, A54+
- Santos, N. C., Mayor, M., Naef, D., et al. 2000, A&A, 361, 265
- Santos, N. C., Mortier, A., Faria, J. P., et al. 2014, A&A, 566, A35
- Vaughan, A. H. & Preston, G. W. 1980, PASP, 92, 385
- Vaughan, A. H., Preston, G. W., & Wilson, O. C. 1978, PASP, 90, 267
- Walkowicz, L. M. & Hawley, S. L. 2009, AJ, 137, 3297

**Appendix A: Plots of the  $S_{H\alpha W}$  analysis**


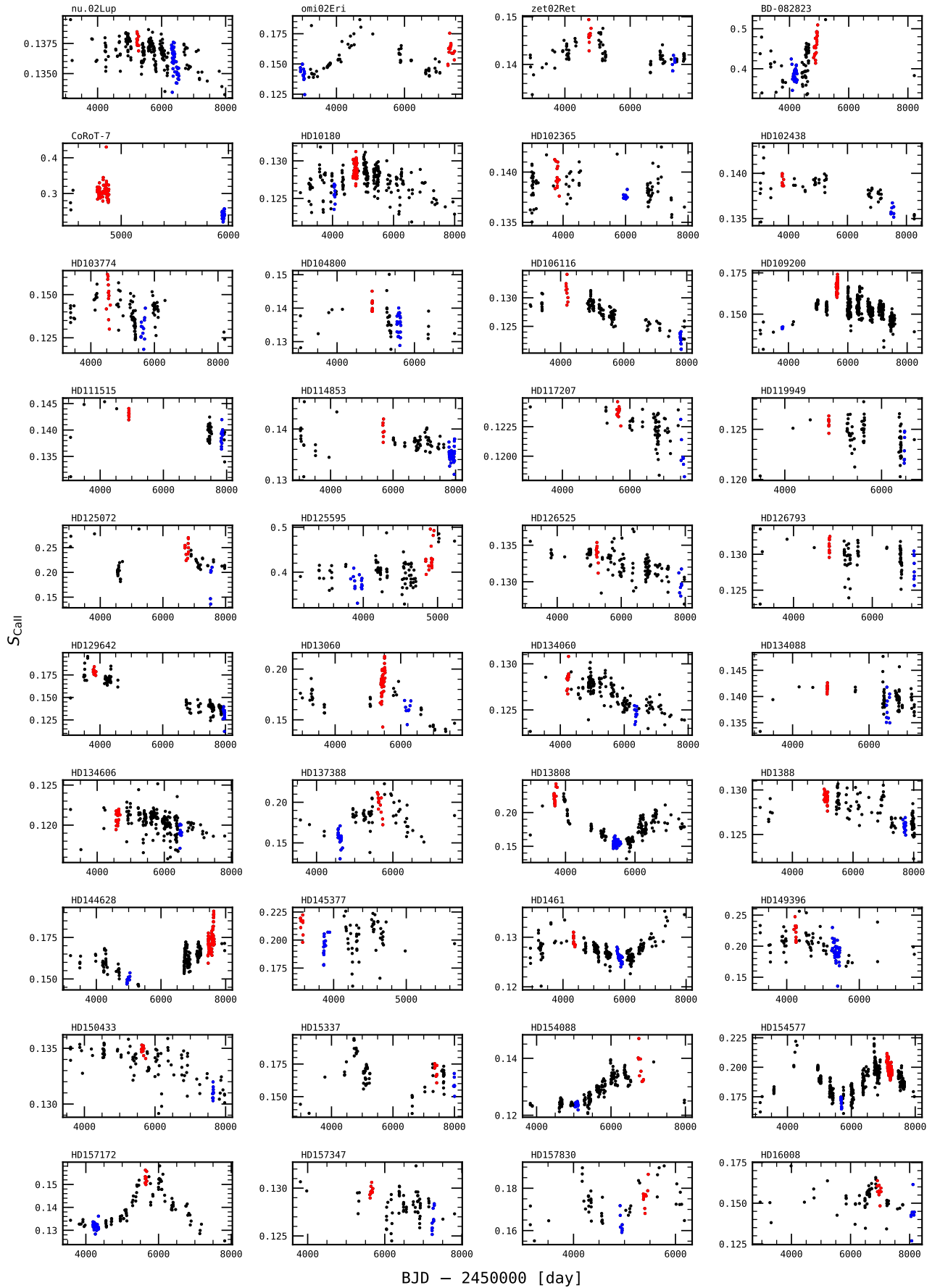
**Fig. A.1.** Spearman correlation coefficient between  $S_{CaII}$  and  $S_{H\alpha 06}$  (black circles) and  $S_{CaII}$  and  $S_{H\alpha W}$  (green triangles) against effective temperature (top panel), metallicity (middle panel), and median  $\log R'_{HK}$ . Horizontal dotted lines mark the thresholds for strong correlations at  $\rho = 0.5$  and  $-0.5$ . Filled markers are significant correlations with  $p$ -value  $\leq 10^{-3}$ .



**Fig. A.2.**  $S_{\text{CaII}}$ ,  $S_{\text{H}\alpha 16}$ , and  $S_{\text{H}\alpha W}$  for HD 215152 (top panels), HD 20003 (middle panels), and HD 7199 (lower panels).

## Appendix B: Ca II time series and selection of maxima and minima

Figure B.1 shows the Ca II time series for the 103 stars used in the short-term analysis in §6. Red and blue points mark the subsets used to calculate correlations at the higher and lower levels of activity, respectively.



**Fig. B.1.**  $S_{\text{CaII}}$  time series. Red points are the epoch at maximum, and blue points are the epoch at minimum.

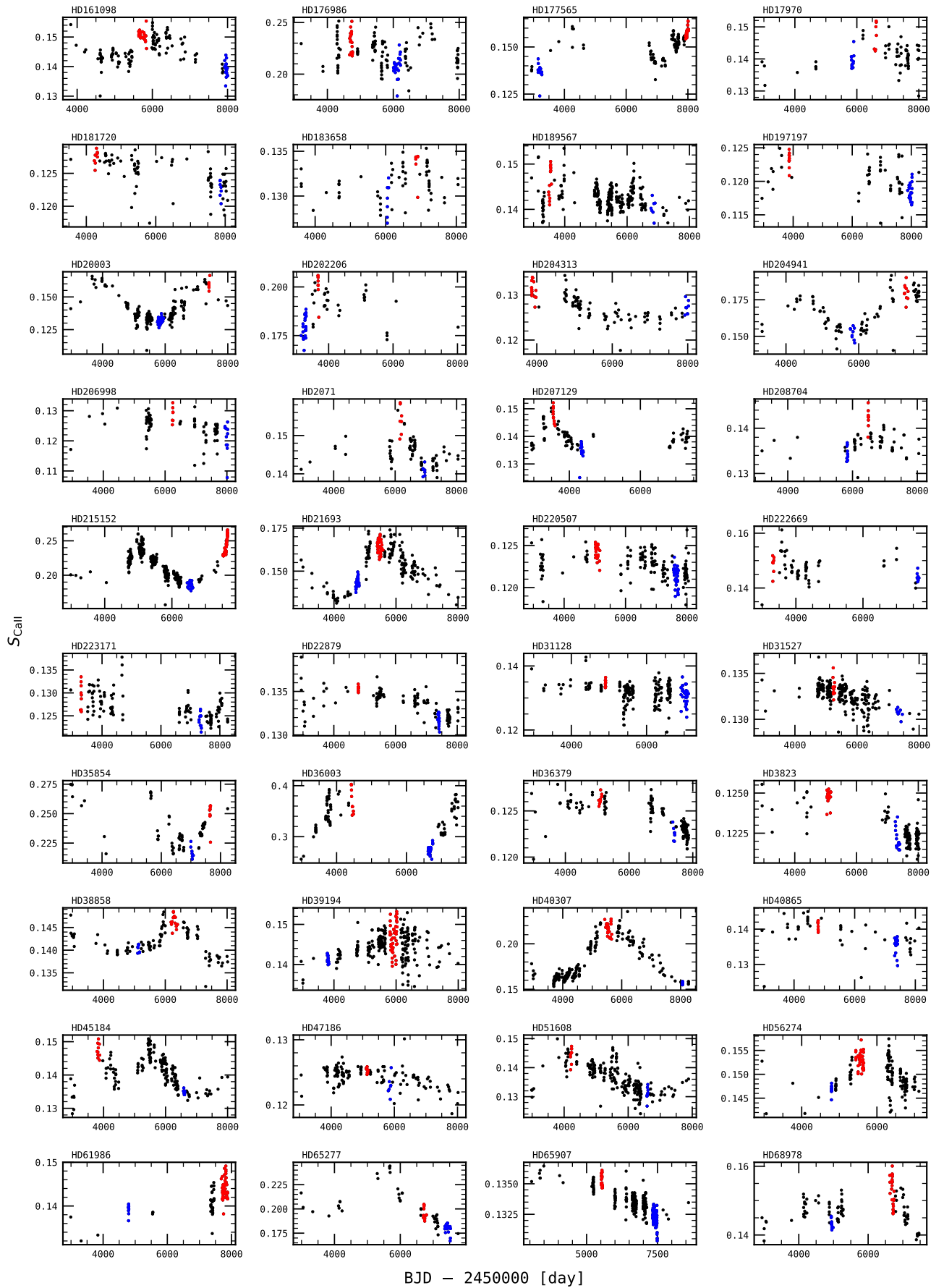


Fig. B.1. continued.

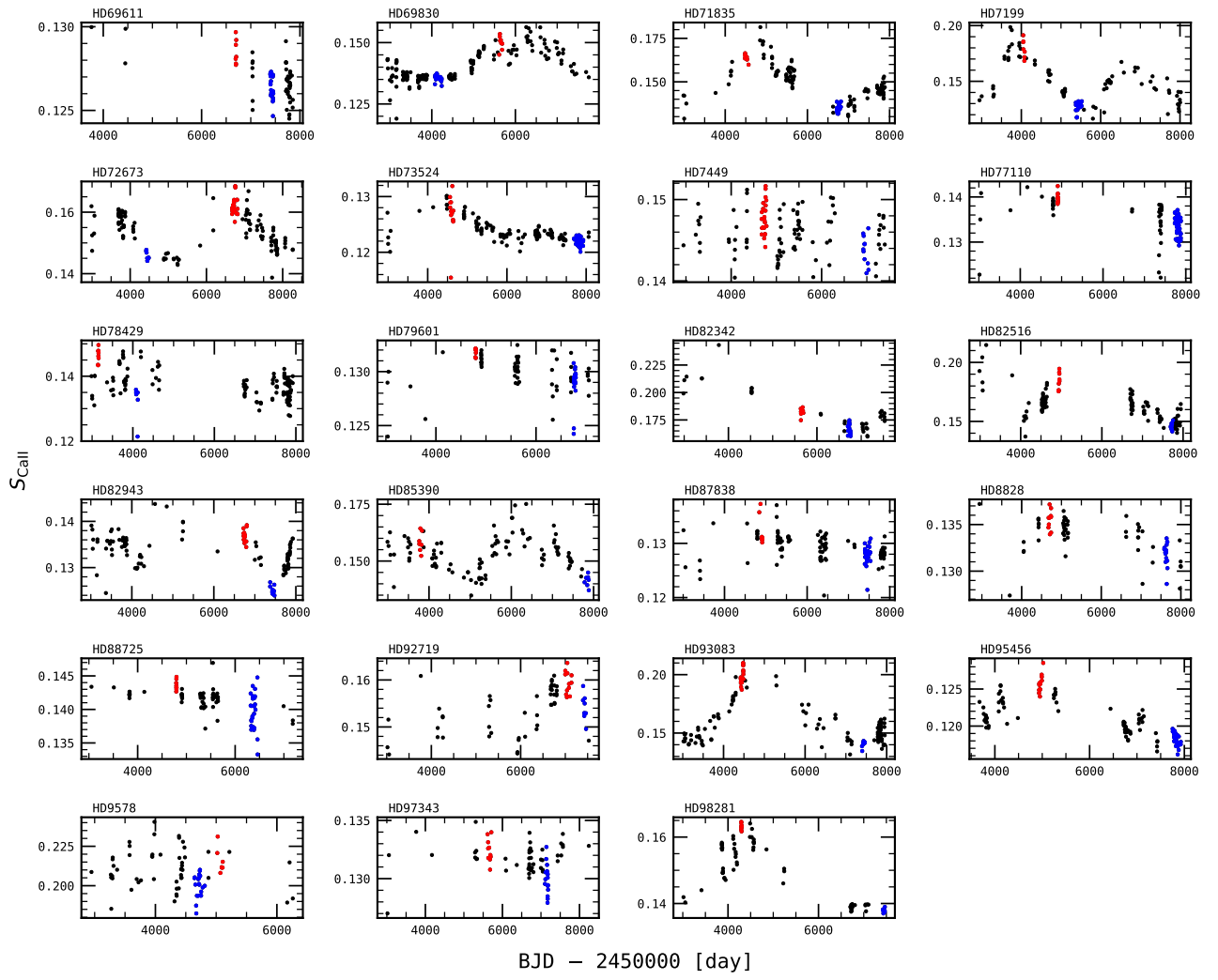


Fig. B.1. continued.

## Appendix C: Tables of stellar parameters and correlations



**Table C.1.** Stellar parameters for the sample.

Star	$N_{\text{nights}}$	$T_{\text{span}}$ [days]	Sp.Type	$T_{\text{eff}}$ [K]	[Fe/H] [dex]	$\langle \log R'_{\text{HK}} \rangle$ [dex]
18 Pup	70	2740	F5	6427 ± 44	0.07 ± 0.03	-4.862 ± 0.004
nu.02 Lup	246	4815	G5	5664 ± 14	-0.34 ± 0.01	-4.941 ± 0.007
omi02 Eri	96	4530	K2	5072 ± 53	-0.42 ± 0.04	-4.961 ± 0.045
zet02 Ret	99	4723	G2	5824 ± 15	-0.22 ± 0.01	-4.875 ± 0.014
BD-08 2823	106	5209	K4	4672 ± 104	-0.04 ± 0.06	-4.685 ± 0.039
CoRoT-7	97	1437	K0	5288 ± 27	0.02 ± 0.02	-4.807 ± 0.046
HD 10180	268	5048	G0	5911 ± 19	0.08 ± 0.01	-4.994 ± 0.013
HD 101930	73	4528	K1	5164 ± 61	0.13 ± 0.04	-4.998 ± 0.040
HD 102117	71	4509	G5	5657 ± 24	0.28 ± 0.02	-5.126 ± 0.017
HD 102365	102	4934	G5	5629 ± 29	-0.29 ± 0.02	-4.949 ± 0.009
HD 102438	66	5228	G7	5560 ± 13	-0.29 ± 0.01	-4.949 ± 0.010
HD 103774	115	4850	F3	6732 ± 56	0.29 ± 0.03	-4.764 ± 0.050
HD 104067	87	2271	K2	4969 ± 72	-0.06 ± 0.05	-4.735 ± 0.025
HD 104800	62	3984	G4	5697 ± 25	-0.79 ± 0.02	-4.886 ± 0.025
HD 106116	134	4888	G4	5680 ± 15	0.14 ± 0.01	-5.030 ± 0.018
HD 107094	76	5155	G6	5562 ± 17	-0.51 ± 0.01	-4.825 ± 0.028
HD 109200	458	5195	K2	5056 ± 33	-0.35 ± 0.02	-4.956 ± 0.027
HD 109271	99	4807	G2	5783 ± 18	0.10 ± 0.01	-4.996 ± 0.048
HD 111515	64	4876	G9	5398 ± 18	-0.61 ± 0.01	-4.957 ± 0.014
HD 111777	107	4808	G5	5666 ± 19	-0.68 ± 0.01	-4.912 ± 0.013
HD 11397	69	5091	G6	5564 ± 26	-0.54 ± 0.02	-4.898 ± 0.021
HD 114853	127	4934	G3	5705 ± 14	-0.23 ± 0.01	-4.944 ± 0.014
HD 117207	78	4565	G5	5667 ± 21	0.22 ± 0.02	-5.088 ± 0.010
HD 119173	97	4400	G2	5779 ± 44	-0.62 ± 0.03	-4.828 ± 0.018
HD 119949	82	3186	F6	6359 ± 36	-0.41 ± 0.02	-4.904 ± 0.012
HD 125072	71	4919	K3	4794 ± 102	0.24 ± 0.08	-4.930 ± 0.047
HD 125595	113	2075	K4	4636 ± 84	0.09 ± 0.04	-4.761 ± 0.034
HD 126525	130	4814	G5	5638 ± 13	-0.10 ± 0.01	-4.999 ± 0.012
HD 126793	85	3913	G0	5904 ± 33	-0.71 ± 0.02	-4.865 ± 0.013
HD 129642	129	4914	K3	4919 ± 65	-0.09 ± 0.03	-5.047 ± 0.068
HD 13060	90	4702	K0	5255 ± 45	0.02 ± 0.03	-4.851 ± 0.065
HD 133633	68	3076	G6	5571 ± 19	-0.45 ± 0.01	-4.946 ± 0.023
HD 134060	159	4822	G0	5966 ± 14	0.14 ± 0.01	-4.998 ± 0.012
HD 134088	86	4033	G4	5675 ± 22	-0.75 ± 0.02	-4.811 ± 0.013
HD 134606	217	4593	G5	5633 ± 28	0.27 ± 0.02	-5.106 ± 0.010
HD 136713	70	4152	K2	4994 ± 74	0.07 ± 0.05	-4.762 ± 0.036
HD 137388	92	4037	K0	5240 ± 53	0.18 ± 0.03	-4.882 ± 0.054
HD 13808	228	4438	K2	5033 ± 38	-0.21 ± 0.02	-4.905 ± 0.075
HD 1388	147	5082	G0	5954 ± 10	-0.01 ± 0.01	-4.972 ± 0.012
HD 144628	265	4767	K2	5022 ± 26	-0.45 ± 0.02	-4.924 ± 0.027
HD 145377	75	2122	F9	6054 ± 16	0.12 ± 0.01	-4.611 ± 0.035
HD 1461	255	5008	G2	5765 ± 18	0.19 ± 0.01	-5.032 ± 0.013
HD 148211	70	4335	G0	5948 ± 22	-0.62 ± 0.02	-4.901 ± 0.014
HD 149396	104	4249	G5	5657 ± 23	0.19 ± 0.02	-4.683 ± 0.051
HD 150433	112	4366	G5	5665 ± 12	-0.36 ± 0.01	-4.947 ± 0.011
HD 15337	83	5014	K1	5179 ± 44	0.06 ± 0.03	-4.925 ± 0.038
HD 154088	186	4143	G9	5374 ± 43	0.28 ± 0.03	-5.072 ± 0.025
HD 154577	443	4826	K3	4847 ± 35	-0.73 ± 0.01	-4.866 ± 0.030
HD 157172	123	4241	G8	5451 ± 27	0.11 ± 0.02	-5.012 ± 0.042
HD 157347	85	3998	G4	5676 ± 16	0.02 ± 0.01	-5.020 ± 0.011
HD 157830	63	3024	G7	5540 ± 16	-0.25 ± 0.01	-4.788 ± 0.033
HD 16008	76	5215	G2	5770 ± 14	-0.06 ± 0.01	-4.841 ± 0.034
HD 161098	149	4172	G7	5560 ± 15	-0.27 ± 0.01	-4.929 ± 0.026
HD 172568	69	3795	G3	5728 ± 22	-0.37 ± 0.02	-4.910 ± 0.020
HD 175607	111	3912	G9	5392 ± 17	-0.62 ± 0.01	-4.933 ± 0.020
HD 176986	161	4762	K2	5018 ± 59	0.00 ± 0.03	-4.830 ± 0.028
HD 177565	145	5082	G5	5627 ± 19	0.08 ± 0.01	-4.901 ± 0.036
HD 17970	74	5063	K2	5038 ± 31	-0.45 ± 0.02	-5.006 ± 0.019
HD 181433	184	5029	K2	4962 ± 134	0.33 ± 0.13	-5.128 ± 0.016
HD 181720	89	4519	G2	5792 ± 17	-0.53 ± 0.01	-4.978 ± 0.019
HD 183658	72	4446	G2	5803 ± 17	0.03 ± 0.01	-4.941 ± 0.014
HD 189567	256	5031	G3	5726 ± 15	-0.24 ± 0.01	-4.914 ± 0.016
HD 19467	71	5110	G3	5720 ± 10	-0.14 ± 0.01	-5.009 ± 0.009
HD 197027	66	3077	G4	5694 ± 28	0.07 ± 0.02	-5.002 ± 0.020
HD 197197	78	5313	G2	5812 ± 16	-0.46 ± 0.01	-5.024 ± 0.020
HD 199289	64	4012	G0	5928 ± 37	-0.98 ± 0.03	-4.846 ± 0.013
HD 199847	81	5120	G2	5763 ± 20	-0.54 ± 0.02	-5.003 ± 0.025
HD 20003	193	5010	G8	5494 ± 27	0.04 ± 0.02	-5.012 ± 0.057
HD 202206	62	4872	G2	5757 ± 25	0.29 ± 0.02	-4.749 ± 0.035
HD 20407	72	5130	G1	5866 ± 14	-0.44 ± 0.01	-4.878 ± 0.009
HD 204313	106	4158	G2	5776 ± 22	0.18 ± 0.02	-5.043 ± 0.020
HD 204941	96	4312	K2	4997 ± 36	-0.20 ± 0.02	-4.922 ± 0.041
HD 206998	93	5076	G2	5822 ± 26	-0.69 ± 0.02	-4.927 ± 0.025

Table C.1. continued.

Star	$N_{\text{nights}}$	$T_{\text{span}}$ [days]	Sp.Type	$T_{\text{eff}}$ [K]	[Fe/H] [dex]	$\langle \log R'_{\text{HK}} \rangle$ [dex]
HD 2071	83	5104	G3	5719 ± 14	-0.09 ± 0.01	-4.921 ± 0.021
HD 207129	107	4418	G0	5937 ± 13	0.00 ± 0.01	-4.890 ± 0.027
HD 20781	224	5014	K0	5256 ± 29	-0.11 ± 0.02	-5.050 ± 0.013
HD 20782	84	5109	G2	5774 ± 14	-0.06 ± 0.01	-4.907 ± 0.015
HD 207869	80	5034	G7	5527 ± 21	-0.45 ± 0.02	-4.949 ± 0.027
HD 208704	69	4846	G1	5826 ± 11	-0.09 ± 0.01	-4.944 ± 0.017
HD 210918	136	5108	G2	5755 ± 12	-0.09 ± 0.01	-5.012 ± 0.009
HD 21132	92	4245	F7	6243 ± 34	-0.37 ± 0.02	-4.856 ± 0.035
HD 211415	65	4433	G1	5850 ± 14	-0.21 ± 0.01	-4.929 ± 0.016
HD 21209	64	4720	K4	4671 ± 65	-0.41 ± 0.04	-4.799 ± 0.025
HD 215152	323	4671	K3	4803 ± 52	-0.08 ± 0.02	-4.861 ± 0.047
HD 21693	218	5060	G8	5430 ± 26	0.00 ± 0.02	-4.913 ± 0.050
HD 219828	91	3751	G1	5888 ± 14	0.18 ± 0.01	-5.117 ± 0.018
HD 220507	199	5109	G4	5698 ± 17	0.01 ± 0.01	-5.075 ± 0.012
HD 222669	68	4677	G1	5894 ± 17	0.05 ± 0.01	-4.839 ± 0.021
HD 223171	134	5327	G1	5841 ± 18	0.12 ± 0.01	-5.029 ± 0.021
HD 224817	106	4266	G1	5894 ± 22	-0.53 ± 0.02	-4.921 ± 0.014
HD 22879	146	5087	G1	5857 ± 27	-0.83 ± 0.02	-4.878 ± 0.010
HD 31103	72	4770	F9	6078 ± 16	0.09 ± 0.01	-4.623 ± 0.039
HD 31128	210	4170	F8	6096 ± 67	-1.39 ± 0.04	-4.814 ± 0.016
HD 31527	248	5053	G1	5898 ± 13	-0.17 ± 0.01	-4.938 ± 0.008
HD 31822	82	4523	F9	6042 ± 16	-0.19 ± 0.01	-4.821 ± 0.010
HD 32564	189	2301	G7	5533 ± 29	0.01 ± 0.02	-5.030 ± 0.015
HD 35854	77	5298	K3	4928 ± 56	-0.13 ± 0.03	-4.814 ± 0.034
HD 36003	111	4489	K4	4647 ± 88	-0.20 ± 0.06	-4.867 ± 0.050
HD 36379	147	4926	F9	6030 ± 14	-0.17 ± 0.01	-4.951 ± 0.014
HD 3823	137	5081	F9	6022 ± 14	-0.28 ± 0.01	-4.972 ± 0.009
HD 38858	119	5076	G3	5733 ± 12	-0.22 ± 0.01	-4.908 ± 0.018
HD 39194	271	5050	K1	5205 ± 23	-0.61 ± 0.02	-4.962 ± 0.017
HD 40307	253	5324	K2	4977 ± 59	-0.31 ± 0.03	-4.964 ± 0.066
HD 40865	73	5174	G3	5719 ± 16	-0.38 ± 0.01	-4.919 ± 0.021
HD 41248	163	5175	G3	5713 ± 21	-0.37 ± 0.01	-4.881 ± 0.021
HD 4308	145	5081	G5	5644 ± 16	-0.34 ± 0.01	-4.956 ± 0.013
HD 45184	189	5061	G1	5869 ± 14	0.04 ± 0.01	-4.901 ± 0.030
HD 45289	62	4869	G3	5717 ± 18	-0.02 ± 0.01	-5.046 ± 0.008
HD 45364	112	4866	G8	5434 ± 20	-0.17 ± 0.01	-4.979 ± 0.022
HD 47186	145	4966	G4	5675 ± 21	0.23 ± 0.02	-5.070 ± 0.010
HD 51608	217	4899	G9	5358 ± 22	-0.07 ± 0.01	-5.015 ± 0.028
HD 5388	75	5067	F6	6311 ± 33	-0.28 ± 0.02	-4.917 ± 0.039
HD 56274	171	4171	G3	5734 ± 22	-0.54 ± 0.02	-4.831 ± 0.017
HD 564	106	5172	G0	5902 ± 14	-0.20 ± 0.01	-4.847 ± 0.052
HD 59468	163	5301	G6	5618 ± 20	0.03 ± 0.01	-5.008 ± 0.011
HD 59711	68	5144	G3	5722 ± 13	-0.12 ± 0.01	-4.930 ± 0.014
HD 61986	95	4888	G3	5725 ± 20	-0.34 ± 0.02	-4.888 ± 0.018
HD 63765	68	5241	G8	5432 ± 19	-0.16 ± 0.01	-4.726 ± 0.046
HD 65277	69	4767	K4	4701 ± 57	-0.30 ± 0.04	-5.042 ± 0.041
HD 65907	301	5531	G0	5945 ± 16	-0.31 ± 0.01	-4.901 ± 0.008
HD 68978	112	4525	G0	5965 ± 22	0.04 ± 0.02	-4.859 ± 0.025
HD 69611	73	4094	G2	5762 ± 25	-0.58 ± 0.02	-4.957 ± 0.011
HD 69830	264	4817	G9	5402 ± 28	-0.06 ± 0.02	-5.013 ± 0.029
HD 71334	61	4822	G4	5694 ± 13	-0.09 ± 0.01	-4.985 ± 0.010
HD 71835	150	4899	G8	5438 ± 22	-0.04 ± 0.02	-4.955 ± 0.053
HD 7199	125	5075	G9	5386 ± 45	0.28 ± 0.03	-5.014 ± 0.088
HD 72673	158	5281	K0	5243 ± 22	-0.41 ± 0.01	-4.922 ± 0.027
HD 73524	156	5082	F9	6017 ± 13	0.16 ± 0.01	-5.002 ± 0.019
HD 7449	116	4452	F9	6024 ± 13	-0.11 ± 0.01	-4.822 ± 0.015
HD 77110	101	4864	G3	5717 ± 20	-0.50 ± 0.02	-4.929 ± 0.021
HD 78429	136	4940	G2	5760 ± 19	0.09 ± 0.01	-4.952 ± 0.029
HD 79601	85	4023	G2	5825 ± 25	-0.59 ± 0.02	-4.931 ± 0.010
HD 82342	65	4549	K5	4470 ± 21	-0.56 ± 0.10	-4.990 ± 0.040
HD 82516	134	4959	K2	5041 ± 57	0.02 ± 0.03	-4.981 ± 0.043
HD 82943	120	4910	F9	5989 ± 20	0.26 ± 0.01	-4.957 ± 0.027
HD 85390	113	4893	K1	5135 ± 45	-0.09 ± 0.02	-4.964 ± 0.029
HD 87838	152	4872	F8	6118 ± 33	-0.40 ± 0.02	-4.851 ± 0.015
HD 8828	79	5058	G9	5403 ± 25	-0.16 ± 0.02	-5.013 ± 0.012
HD 88725	94	4130	G5	5654 ± 17	-0.64 ± 0.01	-4.882 ± 0.013
HD 89839	79	5147	F6	6314 ± 24	0.04 ± 0.02	-4.937 ± 0.049
HD 90156	127	4925	G6	5599 ± 12	-0.24 ± 0.01	-4.950 ± 0.006
HD 92719	67	4509	G2	5824 ± 16	-0.10 ± 0.01	-4.818 ± 0.026
HD 93083	134	4937	K2	5048 ± 66	0.08 ± 0.04	-5.014 ± 0.066
HD 93385	235	4882	G0	5977 ± 18	0.02 ± 0.01	-4.971 ± 0.008
HD 95456	124	4250	F7	6276 ± 22	0.16 ± 0.02	-4.947 ± 0.022
HD 9578	77	3314	F9	6055 ± 14	0.11 ± 0.01	-4.595 ± 0.037
HD 96423	72	4756	G3	5711 ± 18	0.10 ± 0.01	-5.048 ± 0.008

**Table C.1.** continued.

Star	$N_{\text{nights}}$	$T_{\text{span}}$ [days]	Sp.Type	$T_{\text{eff}}$ [K]	[Fe/H] [dex]	$\langle \log R'_{\text{HK}} \rangle$ [dex]
HD 967	73	5081	G6	$5564 \pm 16$	$-0.68 \pm 0.01$	$-4.906 \pm 0.015$
HD 96700	231	4926	G1	$5845 \pm 13$	$-0.18 \pm 0.01$	$-4.938 \pm 0.008$
HD 97037	63	4791	G1	$5883 \pm 14$	$-0.07 \pm 0.01$	$-4.981 \pm 0.009$
HD 97343	73	5225	G9	$5410 \pm 20$	$-0.06 \pm 0.01$	$-5.037 \pm 0.008$

**Notes.**  $N_{\text{nights}}$  is the number of binned nights of observation,  $T_{\text{span}}$  the number of days between first and last observation, Sp.Type is the spectral type,  $T_{\text{eff}}$  the effective temperature, [Fe/H] the metallicity,  $\langle \log R'_{\text{HK}} \rangle$  the median activity levels where the errors are standard deviations of the time series.

**Table C.2.** Spearman correlation coefficients for the long-term dataset.

Star	$\rho^{06}$	$p\text{-value}^{06}$	$\rho^{16}$	$p\text{-value}^{16}$	$\rho^W$	$p\text{-value}^W$
18 Pup	0.29	0.007	0.11	0.178	-0.08	0.248
nu.02 Lup	-0.22	0.000	0.09	0.086	0.14	0.016
omi02 Eri	0.90	0.000	0.55	0.000	-0.20	0.024
zet02 Ret	0.59	0.000	0.12	0.125	-0.24	0.008
BD-08 2823	0.70	0.000	0.43	0.000	0.04	0.328
CoRoT-7	0.80	0.000	0.73	0.000	0.50	0.000
HD 10180	0.16	0.005	-0.14	0.009	-0.20	0.000
HD 101930	0.66	0.000	0.01	0.465	-0.25	0.018
HD 102117	-0.19	0.052	-0.23	0.027	-0.13	0.140
HD 102365	0.12	0.118	-0.13	0.089	-0.18	0.036
HD 102438	-0.06	0.326	0.17	0.086	0.17	0.087
HD 103774	0.63	0.000	0.52	0.000	-0.07	0.222
HD 104067	0.86	0.000	0.26	0.008	-0.22	0.020
HD 104800	0.16	0.103	0.05	0.354	0.00	0.493
HD 106116	-0.28	0.001	-0.50	0.000	-0.48	0.000
HD 107094	0.50	0.000	0.58	0.000	0.43	0.000
HD 109200	0.82	0.000	0.38	0.000	-0.08	0.053
HD 109271	0.18	0.036	-0.05	0.321	-0.12	0.113
HD 111515	-0.19	0.069	-0.11	0.202	-0.12	0.173
HD 111777	-0.25	0.005	-0.30	0.001	-0.26	0.003
HD 11397	-0.02	0.423	0.37	0.001	0.41	0.000
HD 114853	0.16	0.038	-0.13	0.068	-0.20	0.013
HD 117207	-0.32	0.002	0.10	0.198	0.20	0.038
HD 119173	-0.22	0.014	0.03	0.397	0.12	0.130
HD 119949	0.05	0.333	0.08	0.238	0.03	0.393
HD 125072	0.58	0.000	-0.72	0.000	-0.86	0.000
HD 125595	0.70	0.000	0.34	0.000	0.08	0.197
HD 126525	-0.13	0.064	-0.13	0.064	-0.11	0.106
HD 126793	-0.23	0.015	0.03	0.376	0.10	0.187
HD 129642	0.75	0.000	-0.35	0.000	-0.70	0.000
HD 13060	0.80	0.000	0.36	0.000	-0.22	0.018
HD 133633	-0.37	0.001	-0.17	0.086	-0.02	0.425
HD 134060	-0.12	0.063	-0.33	0.000	-0.34	0.000
HD 134088	-0.36	0.000	-0.19	0.037	-0.04	0.360
HD 134606	-0.03	0.306	-0.04	0.290	-0.01	0.421
HD 136713	0.81	0.000	-0.26	0.018	-0.68	0.000
HD 137388	0.73	0.000	0.06	0.274	-0.37	0.000
HD 13808	0.91	0.000	0.75	0.000	-0.32	0.000
HD 1388	0.02	0.384	0.06	0.251	-0.01	0.462
HD 144628	0.91	0.000	0.64	0.000	-0.08	0.104
HD 145377	0.53	0.000	0.60	0.000	0.48	0.000
HD 1461	0.44	0.000	-0.16	0.006	-0.27	0.000
HD 148211	0.08	0.246	0.06	0.320	0.04	0.384
HD 149396	0.58	0.000	0.26	0.004	-0.14	0.085
HD 150433	-0.26	0.003	-0.43	0.000	-0.47	0.000
HD 15337	0.48	0.000	-0.26	0.011	-0.48	0.000
HD 154088	0.60	0.000	-0.35	0.000	-0.52	0.000
HD 154577	0.93	0.000	0.80	0.000	0.22	0.000
HD 157172	0.86	0.000	-0.34	0.000	-0.74	0.000
HD 157347	0.04	0.359	-0.05	0.323	-0.07	0.263
HD 157830	0.93	0.000	0.82	0.000	0.42	0.001
HD 16008	0.65	0.000	0.33	0.003	-0.04	0.372
HD 161098	0.74	0.000	0.25	0.001	-0.46	0.000
HD 172568	-0.27	0.013	-0.35	0.002	-0.31	0.006
HD 175607	0.09	0.171	0.24	0.005	0.19	0.022
HD 176986	0.52	0.000	0.00	0.497	-0.29	0.000
HD 177565	0.91	0.000	0.60	0.000	0.16	0.028
HD 17970	0.53	0.000	-0.02	0.418	-0.34	0.002
HD 181433	0.04	0.287	0.02	0.394	0.01	0.467
HD 181720	-0.07	0.248	-0.15	0.076	-0.06	0.285
HD 183658	0.16	0.085	-0.14	0.121	-0.19	0.055
HD 189567	0.65	0.000	0.40	0.000	0.13	0.017
HD 19467	-0.01	0.461	0.29	0.007	0.30	0.007
HD 197027	-0.26	0.019	-0.14	0.134	-0.04	0.377
HD 197197	-0.26	0.010	-0.40	0.000	-0.32	0.002
HD 199289	0.03	0.408	-0.08	0.271	-0.17	0.082
HD 199847	-0.31	0.004	-0.41	0.000	-0.33	0.001
HD 20003	0.71	0.000	-0.06	0.201	-0.63	0.000
HD 202206	0.89	0.000	0.53	0.000	0.10	0.210
HD 20407	0.05	0.323	0.06	0.311	0.04	0.382
HD 204313	0.54	0.000	-0.20	0.022	-0.41	0.000
HD 204941	0.89	0.000	0.74	0.000	-0.27	0.004
HD 206998	-0.66	0.000	-0.66	0.000	-0.58	0.000
HD 2071	0.85	0.000	0.58	0.000	0.01	0.478

Table C.2. continued.

Star	$\rho^{06}$	$p$ -value <sup>06</sup>	$\rho^{16}$	$p$ -value <sup>16</sup>	$\rho^W$	$p$ -value <sup>W</sup>
HD 207129	0.89	0.000	0.29	0.001	-0.44	0.000
HD 20781	0.01	0.461	0.05	0.207	0.06	0.174
HD 20782	0.45	0.000	0.34	0.001	0.14	0.103
HD 207869	-0.29	0.005	-0.09	0.203	0.04	0.375
HD 208704	0.62	0.000	-0.01	0.461	-0.17	0.078
HD 210918	-0.23	0.004	-0.16	0.028	-0.14	0.050
HD 21132	0.14	0.091	-0.12	0.123	-0.15	0.079
HD 211415	0.54	0.000	-0.25	0.022	-0.43	0.000
HD 21209	0.79	0.000	0.38	0.001	-0.21	0.051
HD 215152	0.96	0.000	0.74	0.000	0.16	0.002
HD 21693	0.91	0.000	0.06	0.182	-0.66	0.000
HD 219828	0.04	0.361	-0.05	0.319	-0.09	0.199
HD 220507	-0.10	0.090	-0.08	0.134	-0.02	0.377
HD 222669	0.65	0.000	0.19	0.061	-0.01	0.451
HD 223171	0.43	0.000	-0.17	0.024	-0.38	0.000
HD 224817	-0.10	0.151	0.07	0.243	0.08	0.211
HD 22879	-0.31	0.000	-0.14	0.052	-0.09	0.142
HD 31103	0.42	0.000	0.47	0.000	0.38	0.001
HD 31128	-0.23	0.001	0.01	0.437	0.12	0.041
HD 31527	0.08	0.105	0.01	0.446	-0.02	0.382
HD 31822	0.34	0.001	0.24	0.015	0.12	0.144
HD 32564	-0.04	0.290	-0.02	0.379	-0.01	0.452
HD 35854	0.94	0.000	0.56	0.000	0.10	0.180
HD 36003	0.89	0.000	0.08	0.202	-0.58	0.000
HD 36379	0.18	0.013	-0.13	0.064	-0.21	0.006
HD 3823	-0.18	0.016	-0.13	0.065	-0.07	0.196
HD 38858	0.55	0.000	-0.01	0.471	-0.41	0.000
HD 39194	0.52	0.000	0.30	0.000	-0.04	0.263
HD 40307	0.93	0.000	0.42	0.000	-0.46	0.000
HD 40865	0.24	0.022	-0.42	0.000	-0.47	0.000
HD 41248	0.29	0.000	0.12	0.065	-0.05	0.256
HD 4308	0.34	0.000	0.01	0.429	-0.13	0.057
HD 45184	0.92	0.000	0.05	0.251	-0.54	0.000
HD 45289	0.26	0.020	0.25	0.026	0.15	0.118
HD 45364	0.39	0.000	-0.20	0.015	-0.34	0.000
HD 47186	-0.14	0.044	-0.13	0.065	-0.10	0.106
HD 51608	0.60	0.000	-0.09	0.093	-0.33	0.000
HD 5388	-0.10	0.196	-0.03	0.402	-0.00	0.486
HD 56274	0.62	0.000	0.71	0.000	0.40	0.000
HD 564	0.33	0.000	0.14	0.075	-0.06	0.277
HD 59468	0.37	0.000	-0.27	0.000	-0.37	0.000
HD 59711	0.61	0.000	0.28	0.013	0.14	0.129
HD 61986	0.67	0.000	0.29	0.003	-0.43	0.000
HD 63765	0.90	0.000	0.76	0.000	0.38	0.001
HD 65277	0.86	0.000	0.39	0.001	-0.35	0.002
HD 65907	0.01	0.410	-0.25	0.000	-0.25	0.000
HD 68978	0.79	0.000	0.41	0.000	-0.27	0.002
HD 69611	-0.18	0.067	-0.33	0.003	-0.32	0.004
HD 69830	0.56	0.000	-0.09	0.068	-0.49	0.000
HD 71334	0.18	0.079	0.10	0.228	0.07	0.285
HD 71835	0.93	0.000	0.13	0.052	-0.67	0.000
HD 7199	0.67	0.000	-0.80	0.000	-0.85	0.000
HD 72673	0.93	0.000	0.52	0.000	-0.25	0.001
HD 73524	0.22	0.003	-0.44	0.000	-0.46	0.000
HD 7449	0.77	0.000	0.46	0.000	-0.14	0.064
HD 77110	-0.20	0.020	-0.22	0.013	-0.20	0.024
HD 78429	0.51	0.000	-0.09	0.156	-0.48	0.000
HD 79601	0.24	0.016	-0.03	0.401	-0.09	0.201
HD 82342	0.55	0.000	-0.26	0.018	-0.51	0.000
HD 82516	0.80	0.000	-0.47	0.000	-0.67	0.000
HD 82943	0.74	0.000	-0.54	0.000	-0.67	0.000
HD 85390	0.72	0.000	0.19	0.023	-0.19	0.022
HD 87838	-0.19	0.009	0.01	0.445	0.07	0.205
HD 8828	-0.30	0.004	-0.16	0.081	-0.08	0.251
HD 88725	0.10	0.161	-0.15	0.080	-0.15	0.080
HD 89839	0.04	0.355	0.07	0.263	0.04	0.352
HD 90156	-0.02	0.396	0.02	0.416	0.01	0.446
HD 92719	0.91	0.000	0.72	0.000	0.26	0.016
HD 93083	0.63	0.000	-0.27	0.001	-0.54	0.000
HD 93385	-0.07	0.153	-0.07	0.155	-0.03	0.349
HD 95456	0.69	0.000	-0.67	0.000	-0.78	0.000
HD 9578	0.52	0.000	0.45	0.000	0.34	0.002
HD 96423	0.15	0.106	0.11	0.172	0.07	0.281
HD 967	0.01	0.462	-0.08	0.252	-0.10	0.202
HD 96700	0.09	0.085	-0.14	0.018	-0.17	0.007

**Table C.2.** continued.

Star	$\rho^{06}$	$p\text{-value}^{06}$	$\rho^{16}$	$p\text{-value}^{16}$	$\rho^W$	$p\text{-value}^W$
HD 97037	0.08	0.255	0.01	0.457	-0.01	0.479
HD 97343	0.08	0.252	-0.05	0.330	-0.03	0.390

**Notes.**  $\rho^{06}$ ,  $\rho^{16}$ , and  $\rho^W$  are the correlation coefficients between  $S_{\text{CaII}}$  and  $S_{\text{H}\alpha 06}$ ,  $S_{\text{H}\alpha 16}$ , and  $S_{\text{H}\alpha W}$ , respectively.  $p\text{-value}$  is the probability of having an equal or higher correlation coefficient (see text).  $p\text{-values}$  of 0.000 means that the value is lower than  $10^{-3}$ .

**Table C.3.** Spearman correlation coefficients for the short-term dataset.

Star	$\langle S_{\text{Call}} \rangle_{\text{max}}$	$\langle S_{\text{Call}} \rangle_{\text{min}}$	$\sigma(S_{\text{Call}})_{\text{max}}$	$\sigma(S_{\text{Call}})_{\text{min}}$	$\rho_{\text{max}}^{06}$	$p\text{-value}_{\text{max}}^{06}$	$\rho_{\text{min}}^{06}$	$p\text{-value}_{\text{min}}^{06}$	$\rho_{\text{max}}^{16}$	$p\text{-value}_{\text{max}}^{16}$	$\rho_{\text{min}}^{16}$	$p\text{-value}_{\text{min}}^{16}$
18 Pup	0.1255	0.1248	0.0004	0.0004	-0.34	0.087	0.27	0.183	-0.20	0.215	0.66	0.013
nu.02 Lup	0.1377	0.1360	0.0004	0.0010	-0.21	0.256	-0.46	0.002	0.14	0.334	0.12	0.223
omi02 Eri	0.1615	0.1421	0.0063	0.0063	0.92	0.000	0.54	0.029	0.59	0.010	0.21	0.235
zet02 Ret	0.1461	0.1402	0.0017	0.0012	0.32	0.186	0.43	0.147	-0.27	0.224	0.21	0.298
BD-08 2823	0.4608	0.3858	0.0257	0.0165	-0.03	0.439	0.08	0.340	0.12	0.286	0.10	0.311
CoRoT-7	0.3072	0.2383	0.0208	0.0094	0.51	0.000	0.50	0.007	0.45	0.000	0.36	0.038
HD 10180	0.1288	0.1257	0.0009	0.0011	-0.12	0.208	0.22	0.250	-0.01	0.474	0.09	0.392
HD 101930	0.1580	0.1482	0.0037	0.0061	-0.12	0.371	0.48	0.076	0.27	0.224	0.18	0.298
HD 102117	0.1168	0.1168	0.0006	0.0006	0.68	0.027	0.68	0.027	-0.08	0.407	-0.08	0.406
HD 102365	0.1395	0.1376	0.0010	0.0003	0.60	0.011	0.10	0.389	-0.18	0.241	-0.10	0.388
HD 102438	0.1392	0.1359	0.0005	0.0005	0.26	0.243	0.64	0.057	0.19	0.308	0.00	0.500
HD 103774	0.1492	0.1302	0.0091	0.0061	-0.03	0.454	0.48	0.054	0.59	0.020	0.32	0.142
HD 104067	0.3071	0.2876	0.0194	0.0162	0.90	0.008	0.67	0.002	0.33	0.187	0.42	0.032
HD 104800	0.1408	0.1352	0.0019	0.0030	0.20	0.287	-0.17	0.206	0.17	0.320	0.05	0.399
HD 106116	0.1312	0.1228	0.0016	0.0010	0.70	0.024	-0.04	0.439	0.85	0.008	0.47	0.045
HD 107094	0.1603	0.1581	0.0067	0.0032	-0.01	0.489	0.16	0.220	-0.07	0.395	0.27	0.105
HD 109200	0.1665	0.1417	0.0036	0.0003	0.79	0.000	-0.23	0.254	0.31	0.021	-0.17	0.319
HD 109271	0.1391	0.1255	0.0092	0.0068	0.35	0.075	0.12	0.235	0.30	0.108	-0.21	0.099
HD 111515	0.1430	0.1388	0.0006	0.0013	-0.02	0.481	-0.09	0.359	0.47	0.091	-0.07	0.389
HD 111777	0.1374	0.1365	0.0020	0.0025	-0.20	0.052	0.10	0.400	-0.31	0.007	-0.69	0.034
HD 11397	0.1519	0.1468	0.0016	0.0077	0.49	0.020	-0.07	0.378	0.35	0.072	0.22	0.170
HD 114853	0.1398	0.1350	0.0015	0.0013	-0.50	0.109	0.18	0.114	-0.14	0.363	0.04	0.386
HD 117207	0.1237	0.1202	0.0005	0.0015	-0.39	0.107	-0.61	0.069	-0.05	0.443	0.46	0.128
HD 119173	0.1413	0.1380	0.0008	0.0044	0.43	0.147	0.03	0.446	0.32	0.214	0.18	0.186
HD 119949	0.1256	0.1232	0.0005	0.0013	-0.86	0.018	-0.54	0.092	-0.07	0.431	-0.14	0.362
HD 125072	0.2464	0.1862	0.0138	0.0285	0.69	0.004	-0.54	0.094	-0.37	0.087	-0.86	0.018
HD 125595	0.4329	0.3757	0.0286	0.0178	0.48	0.024	0.52	0.032	-0.37	0.062	0.42	0.069
HD 126525	0.1338	0.1297	0.0011	0.0013	0.33	0.159	0.68	0.049	0.20	0.275	0.14	0.364
HD 126793	0.1310	0.1282	0.0009	0.0017	0.16	0.300	-0.90	0.008	0.10	0.375	-0.71	0.031
HD 129642	0.1784	0.1316	0.0029	0.0063	0.37	0.152	-0.19	0.240	0.47	0.093	-0.62	0.010
HD 13060	0.1880	0.1607	0.0134	0.0066	0.60	0.000	0.03	0.462	0.11	0.240	-0.18	0.302
HD 133633	0.1375	0.1365	0.0028	0.0020	-0.24	0.105	0.07	0.388	-0.31	0.054	-0.32	0.093
HD 134060	0.1283	0.1246	0.0010	0.0006	-0.32	0.157	-0.68	0.019	0.38	0.115	-0.30	0.186
HD 134088	0.1416	0.1378	0.0006	0.0023	0.20	0.287	-0.76	0.012	-0.38	0.139	-0.66	0.024
HD 134606	0.1211	0.1191	0.0007	0.0008	0.24	0.111	0.14	0.338	-0.25	0.104	0.25	0.230
HD 136713	0.2841	0.2744	0.0164	0.0145	0.87	0.001	0.77	0.010	0.54	0.030	0.24	0.240
HD 137388	0.1972	0.1559	0.0117	0.0086	0.38	0.101	0.39	0.035	-0.27	0.181	0.62	0.002
HD 13808	0.2228	0.1555	0.0088	0.0037	0.73	0.001	0.36	0.003	0.72	0.001	-0.16	0.114
HD 1388	0.1291	0.1259	0.0006	0.0005	0.49	0.011	0.08	0.361	0.28	0.096	0.06	0.391
HD 144628	0.1738	0.1495	0.0071	0.0021	0.76	0.000	0.60	0.047	0.85	0.000	0.12	0.372
HD 145377	0.2139	0.1948	0.0075	0.0090	0.67	0.030	0.75	0.002	0.83	0.010	0.56	0.018
HD 1461	0.1293	0.1259	0.0010	0.0008	-0.32	0.135	-0.01	0.486	0.02	0.470	0.20	0.138
HD 148211	0.1302	0.1280	0.0016	0.0023	-0.18	0.300	0.24	0.124	-0.32	0.186	0.19	0.179
HD 149396	0.2230	0.1913	0.0127	0.0159	0.58	0.041	0.28	0.056	0.36	0.142	0.10	0.284
HD 150433	0.1348	0.1310	0.0004	0.0005	0.60	0.034	0.35	0.150	0.18	0.297	0.16	0.311
HD 15337	0.1697	0.1594	0.0047	0.0052	0.57	0.053	0.82	0.022	0.48	0.089	0.50	0.111
HD 154088	0.1369	0.1235	0.0048	0.0007	0.83	0.010	0.15	0.296	0.42	0.120	0.26	0.176
HD 154577	0.1995	0.1710	0.0048	0.0034	0.73	0.000	0.91	0.000	0.82	0.000	0.75	0.001
HD 157172	0.1524	0.1318	0.0021	0.0015	0.38	0.128	0.07	0.364	-0.08	0.407	-0.20	0.164
HD 157347	0.1297	0.1266	0.0004	0.0011	-0.10	0.380	0.04	0.449	-0.70	0.018	-0.22	0.253
HD 157830	0.1762	0.1634	0.0045	0.0042	0.55	0.043	0.86	0.018	0.48	0.065	0.86	0.018
HD 16008	0.1578	0.1434	0.0035	0.0087	0.81	0.003	-0.12	0.376	0.65	0.013	-0.86	0.011
HD 161098	0.1506	0.1391	0.0017	0.0023	0.51	0.009	0.10	0.334	0.47	0.014	0.08	0.367
HD 172568	0.1434	0.1379	0.0011	0.0050	-0.38	0.128	-0.03	0.440	-0.42	0.105	-0.06	0.373
HD 175607	0.1482	0.1421	0.0019	0.0046	0.65	0.026	-0.55	0.075	0.65	0.027	-0.07	0.425
HD 176986	0.2298	0.2072	0.0098	0.0087	0.54	0.007	0.21	0.130	0.44	0.022	-0.05	0.402
HD 177565	0.1577	0.1371	0.0024	0.0038	0.82	0.000	-0.21	0.200	0.45	0.009	-0.30	0.108
HD 17970	0.1470	0.1396	0.0039	0.0023	0.86	0.017	0.25	0.208	0.25	0.269	-0.32	0.157
HD 181433	0.1371	0.1325	0.0037	0.0046	-0.56	0.016	0.29	0.245	0.30	0.133	0.11	0.396
HD 181720	0.1274	0.1226	0.0010	0.0012	-0.31	0.205	0.11	0.398	-0.43	0.130	-0.82	0.022
HD 183658	0.1336	0.1296	0.0015	0.0017	-0.21	0.299	0.75	0.033	-0.21	0.301	0.54	0.097
HD 189567	0.1463	0.1403	0.0033	0.0018	0.74	0.004	0.96	0.010	0.63	0.012	0.29	0.241
HD 19467	0.1292	0.1280	0.0015	0.0001	-0.15	0.335	-0.64	0.057	-0.15	0.335	0.32	0.215
HD 197027	0.1297	0.1265	0.0029	0.0010	-0.34	0.068	-0.14	0.352	-0.48	0.018	0.02	0.475
HD 197197	0.1232	0.1185	0.0010	0.0012	0.35	0.130	-0.08	0.362	0.15	0.311	-0.26	0.123
HD 199289	0.1344	0.1337	0.0011	0.0028	-0.36	0.172	-0.19	0.164	-0.74	0.023	-0.02	0.465
HD 199847	0.1240	0.1214	0.0031	0.0054	-0.64	0.002	0.31	0.112	-0.81	0.000	0.13	0.310
HD 20003	0.1597	0.1315	0.0034	0.0023	0.86	0.018	0.18	0.168	0.68	0.049	0.05	0.395
HD 202206	0.2005	0.1801	0.0066	0.0054	0.67	0.039	0.61	0.002	0.48	0.105	-0.30	0.075
HD 20407	0.1396	0.1376	0.0009	0.0013	-0.03	0.454	0.38	0.100	0.50	0.050	-0.01	0.491
HD 204313	0.1313	0.1272	0.0018	0.0014	0.28	0.129	0.31	0.207	0.30	0.115	0.31	0.207
HD 204941	0.1803	0.1522	0.0053	0.0038	0.33	0.160	0.23	0.254	-0.14	0.337	-0.12	0.370
HD 206998	0.1288	0.1209	0.0024	0.0049	0.36	0.191	-0.15	0.314	0.46	0.130	-0.39	0.106
HD 2071	0.1541	0.1408	0.0033	0.0012	0.93	0.012	0.57	0.081	0.89	0.015	0.36	0.192

Table C.3. continued.

Star	$\langle S_{\text{Call}} \rangle_{\text{max}}$	$\langle S_{\text{Call}} \rangle_{\text{min}}$	$\sigma(S_{\text{Call}})_{\text{max}}$	$\sigma(S_{\text{Call}})_{\text{min}}$	$\rho_{\text{max}}^{\text{06}}$	$p\text{-value}_{\text{max}}^{\text{06}}$	$\rho_{\text{min}}^{\text{06}}$	$p\text{-value}_{\text{min}}^{\text{06}}$	$\rho_{\text{max}}^{\text{16}}$	$p\text{-value}_{\text{max}}^{\text{16}}$	$\rho_{\text{min}}^{\text{16}}$	$p\text{-value}_{\text{min}}^{\text{16}}$
HD 207129	0.1475	0.1347	0.0026	0.0029	0.92	0.002	0.41	0.059	0.66	0.019	0.03	0.459
HD 20781	0.1332	0.1302	0.0009	0.0028	0.07	0.425	-0.22	0.162	-0.20	0.287	-0.16	0.233
HD 20782	0.1421	0.1400	0.0016	0.0012	0.29	0.243	0.75	0.003	0.36	0.188	0.58	0.018
HD 207869	0.1413	0.1360	0.0017	0.0037	0.29	0.223	-0.38	0.067	0.02	0.475	-0.30	0.114
HD 208704	0.1422	0.1345	0.0021	0.0014	0.50	0.092	0.85	0.005	-0.43	0.129	0.02	0.478
HD 210918	0.1286	0.1271	0.0015	0.0007	-0.86	0.017	-0.27	0.152	-0.36	0.191	0.50	0.030
HD 21132	0.1361	0.1313	0.0045	0.0012	0.16	0.283	-0.25	0.136	-0.08	0.394	-0.17	0.237
HD 211415	0.1351	0.1349	0.0005	0.0007	0.13	0.351	0.29	0.243	-0.05	0.443	0.54	0.093
HD 21209	0.3427	0.3223	0.0129	0.0100	0.90	0.001	0.82	0.023	0.42	0.065	0.07	0.432
HD 215152	0.2452	0.1848	0.0118	0.0040	0.95	0.000	0.62	0.002	0.90	0.000	0.46	0.017
HD 21693	0.1640	0.1434	0.0037	0.0027	0.64	0.000	0.39	0.015	0.09	0.285	0.05	0.401
HD 219828	0.1149	0.1136	0.0010	0.0033	-0.06	0.404	0.83	0.009	-0.06	0.392	0.05	0.444
HD 220507	0.1242	0.1213	0.0008	0.0011	0.13	0.275	0.35	0.019	0.46	0.015	0.26	0.065
HD 222669	0.1485	0.1440	0.0030	0.0013	0.68	0.049	0.71	0.016	0.04	0.465	-0.15	0.325
HD 223171	0.1294	0.1241	0.0026	0.0015	-0.30	0.200	0.70	0.013	-0.23	0.253	0.05	0.432
HD 224817	0.1287	0.1267	0.0014	0.0024	0.21	0.228	0.33	0.071	0.44	0.064	0.53	0.010
HD 22879	0.1354	0.1317	0.0003	0.0006	0.07	0.421	0.07	0.390	0.36	0.141	0.24	0.164
HD 31103	0.1894	0.1831	0.0127	0.0138	0.51	0.054	0.50	0.111	0.70	0.013	0.21	0.300
HD 31128	0.1347	0.1308	0.0010	0.0026	0.01	0.493	0.10	0.284	-0.19	0.285	-0.26	0.070
HD 31527	0.1335	0.1307	0.0009	0.0004	-0.15	0.303	0.64	0.045	0.05	0.424	0.55	0.072
HD 31822	0.1446	0.1428	0.0011	0.0010	0.17	0.221	0.64	0.056	0.30	0.093	0.46	0.128
HD 32564	0.1326	0.1304	0.0017	0.0029	-0.13	0.250	-0.23	0.211	-0.13	0.249	0.11	0.351
HD 35854	0.2501	0.2174	0.0084	0.0048	0.65	0.020	0.89	0.013	0.52	0.050	0.82	0.023
HD 36003	0.3687	0.2747	0.0218	0.0082	0.90	0.003	-0.11	0.317	0.81	0.008	-0.35	0.056
HD 36379	0.1263	0.1226	0.0005	0.0007	0.10	0.379	0.36	0.192	-0.42	0.103	-0.07	0.431
HD 3823	0.1248	0.1222	0.0004	0.0006	0.32	0.105	0.13	0.315	-0.19	0.226	0.68	0.006
HD 38858	0.1463	0.1404	0.0014	0.0008	0.80	0.003	0.48	0.104	-0.42	0.072	0.19	0.307
HD 39194	0.1466	0.1412	0.0035	0.0009	0.67	0.000	-0.27	0.176	0.43	0.002	0.13	0.323
HD 40307	0.2163	0.1568	0.0066	0.0013	0.89	0.000	0.36	0.194	0.45	0.026	0.71	0.040
HD 40865	0.1411	0.1357	0.0012	0.0021	0.68	0.021	-0.15	0.252	0.01	0.493	0.28	0.102
HD 41248	0.1452	0.1421	0.0020	0.0042	0.32	0.184	0.18	0.206	-0.07	0.425	0.19	0.200
HD 4308	0.1377	0.1347	0.0015	0.0019	-0.06	0.410	0.15	0.257	0.10	0.358	-0.02	0.464
HD 45184	0.1473	0.1349	0.0020	0.0006	0.87	0.005	0.22	0.249	0.77	0.010	0.24	0.237
HD 45289	0.1254	0.1252	0.0004	0.0006	0.32	0.216	-0.10	0.400	0.57	0.081	-0.07	0.426
HD 45364	0.1444	0.1392	0.0072	0.0020	0.77	0.014	0.55	0.041	0.00	0.500	-0.18	0.282
HD 47186	0.1253	0.1229	0.0003	0.0014	0.38	0.128	-0.18	0.330	-0.42	0.104	-0.71	0.041
HD 51608	0.1441	0.1311	0.0025	0.0020	0.55	0.073	-0.47	0.094	0.76	0.021	0.07	0.425
HD 5388	0.1194	0.1174	0.0054	0.0076	-0.00	0.499	-0.20	0.165	-0.26	0.120	-0.01	0.483
HD 56274	0.1530	0.1468	0.0016	0.0009	0.33	0.028	0.59	0.038	0.67	0.000	-0.14	0.339
HD 564	0.1535	0.1351	0.0113	0.0106	-0.18	0.254	-0.20	0.196	-0.12	0.325	-0.34	0.069
HD 59468	0.1335	0.1307	0.0013	0.0015	0.75	0.013	0.46	0.004	0.94	0.003	-0.57	0.000
HD 59711	0.1382	0.1375	0.0007	0.0015	0.29	0.171	0.75	0.014	-0.18	0.274	0.32	0.169
HD 61986	0.1442	0.1393	0.0021	0.0011	0.38	0.004	0.18	0.298	0.27	0.033	-0.30	0.189
HD 63765	0.2063	0.1975	0.0048	0.0125	0.96	0.001	0.86	0.000	0.85	0.003	0.62	0.001
HD 65277	0.1962	0.1796	0.0062	0.0047	0.55	0.034	0.61	0.005	-0.50	0.048	0.25	0.153
HD 65907	0.1352	0.1322	0.0005	0.0006	0.47	0.013	0.23	0.027	0.14	0.248	0.05	0.336
HD 68978	0.1526	0.1434	0.0042	0.0013	0.89	0.000	0.11	0.364	0.70	0.000	-0.12	0.354
HD 69611	0.1285	0.1264	0.0007	0.0007	-0.43	0.148	0.14	0.267	0.18	0.332	-0.12	0.304
HD 69830	0.1499	0.1356	0.0026	0.0010	0.81	0.016	0.26	0.088	-0.07	0.425	-0.36	0.028
HD 71334	0.1307	0.1306	0.0009	0.0014	0.32	0.215	0.28	0.144	-0.43	0.145	0.06	0.410
HD 71835	0.1640	0.1346	0.0018	0.0021	-0.30	0.199	0.41	0.042	0.67	0.031	0.18	0.218
HD 7199	0.1796	0.1283	0.0076	0.0033	0.86	0.018	0.04	0.398	-0.64	0.057	-0.11	0.263
HD 72673	0.1619	0.1459	0.0025	0.0014	0.71	0.000	0.25	0.239	0.35	0.040	-0.20	0.285
HD 73524	0.1270	0.1219	0.0037	0.0007	-0.42	0.074	-0.22	0.102	0.10	0.358	0.23	0.093
HD 7449	0.1478	0.1438	0.0020	0.0017	0.73	0.000	0.68	0.015	0.75	0.000	0.19	0.273
HD 77110	0.1399	0.1337	0.0011	0.0020	0.14	0.337	-0.09	0.263	0.08	0.408	-0.20	0.080
HD 78429	0.1464	0.1327	0.0020	0.0047	-0.31	0.206	-0.18	0.332	-0.48	0.105	-0.64	0.060
HD 79601	0.1318	0.1290	0.0003	0.0015	-0.86	0.018	0.16	0.229	-0.39	0.166	0.19	0.196
HD 82342	0.1824	0.1670	0.0031	0.0042	-0.41	0.112	0.17	0.233	0.32	0.166	-0.45	0.024
HD 82516	0.1840	0.1461	0.0067	0.0026	0.67	0.030	-0.34	0.143	0.52	0.071	-0.01	0.489
HD 82943	0.1370	0.1252	0.0013	0.0009	0.64	0.013	0.38	0.124	-0.02	0.470	0.50	0.066
HD 85390	0.1583	0.1413	0.0040	0.0024	0.86	0.017	-0.04	0.465	0.57	0.082	-0.54	0.094
HD 87838	0.1318	0.1279	0.0022	0.0016	0.00	0.500	0.00	0.499	0.50	0.050	0.08	0.322
HD 8828	0.1355	0.1319	0.0010	0.0012	0.34	0.143	-0.02	0.473	-0.09	0.387	-0.05	0.419
HD 88725	0.1436	0.1394	0.0007	0.0026	-0.57	0.066	0.12	0.271	-0.43	0.132	-0.03	0.436
HD 89839	0.1251	0.1192	0.0086	0.0022	0.01	0.488	0.10	0.377	0.06	0.406	-0.10	0.376
HD 90156	0.1385	0.1375	0.0005	0.0011	-0.43	0.030	-0.15	0.312	0.28	0.116	0.30	0.173
HD 92719	0.1595	0.1542	0.0023	0.0026	0.85	0.002	0.95	0.006	0.68	0.012	0.74	0.026
HD 93083	0.1982	0.1405	0.0066	0.0025	0.29	0.131	-0.69	0.035	-0.38	0.071	-0.43	0.129
HD 93385	0.1273	0.1255	0.0004	0.0014	-0.51	0.040	-0.62	0.031	-0.14	0.310	-0.59	0.039
HD 95456	0.1257	0.1183	0.0011	0.0008	0.69	0.004	0.06	0.355	-0.51	0.025	0.14	0.207
HD 9578	0.2157	0.1997	0.0073	0.0071	0.46	0.128	-0.06	0.402	0.75	0.034	-0.13	0.280
HD 96423	0.1263	0.1247	0.0007	0.0013	0.13	0.328	-0.22	0.245	-0.24	0.209	0.15	0.326
HD 967	0.1441	0.1418	0.0005	0.0023	0.75	0.013	0.78	0.001	0.62	0.031	0.16	0.255
HD 96700	0.1346	0.1324	0.0012	0.0011	0.37	0.015	-0.20	0.131	-0.10	0.277	-0.13	0.230



**Table C.3.** continued.

Star	$\langle S_{\text{CaII}} \rangle_{\text{max}}$	$\langle S_{\text{CaII}} \rangle_{\text{min}}$	$\sigma(S_{\text{CaII}})_{\text{max}}$	$\sigma(S_{\text{CaII}})_{\text{min}}$	$\rho_{\text{max}}^{06}$	$p\text{-value}_{\text{max}}^{06}$	$\rho_{\text{min}}^{06}$	$p\text{-value}_{\text{min}}^{06}$	$\rho_{\text{max}}^{16}$	$p\text{-value}_{\text{max}}^{16}$	$\rho_{\text{min}}^{16}$	$p\text{-value}_{\text{min}}^{16}$
HD 97037	0.1279	0.1263	0.0008	0.0011	-0.05	0.435	-0.35	0.067	-0.71	0.017	-0.23	0.166
HD 97343	0.1324	0.1300	0.0010	0.0012	0.52	0.061	0.10	0.349	-0.05	0.435	0.54	0.019

**Notes.**  $\langle S_{\text{CaII}} \rangle$  is the mean  $S_{\text{CaII}}$ ,  $\rho^{06}$ ,  $\rho^{16}$  are the correlation coefficients between  $S_{\text{CaII}}$  and  $S_{\text{H}\alpha 06}$ , and  $S_{\text{H}\alpha 16}$ , respectively.  $p\text{-value}$  is the probability of having an equal or higher correlation coefficient (see text).  $p\text{-values}$  of 0.000 means that the value is lower than  $10^{-3}$ . The subscripts 'max' and 'min', refer to the short-term correlations at epochs when the star is at maximum and minimum of activity, respectively.